Inorganic Chemistry

Article

pubs.acs.org/IC

Strong and Anisotropic Superexchange in the Single-Molecule Magnet (SMM) $[Mn^{III}_6Os^{III}]^{3+}$: Promoting SMM Behavior through 3d–5d Transition Metal Substitution

Veronika Hoeke,[†] Anja Stammler,[†] Hartmut Bögge,[†] Jürgen Schnack,*[,‡] and Thorsten Glaser*[,†]

[†]Lehrstuhl für Anorganische Chemie I, Fakultät für Chemie, Universität Bielefeld, Universitätsstraße 25, D-33615 Bielefeld, Germany

[‡]Fakultät für Physik, Universität Bielefeld, Universitätsstraße 25, D-33615 Bielefeld, Germany

Supporting Information

ABSTRACT: The reaction of the *in situ* generated trinuclear triplesalen complex $[(talen^{t\text{-}Bu_2})Mn^{III}_3(solv)_n]^{3+}$ with $(Ph_4P)_3[Os^{III}(CN)_6]$ and $NaClO_4{\cdot}H_2O$ affords $[\mathbf{Mn^{III}_6Os^{III}}](ClO_4)_3$ (= $[\{(talen^{t\text{-}Bu_2})Mn^{III}_3\}_2\{Os^{III}(CN)_6\}](ClO_4)_3$) in the presence of the oxidizing agent $[(tacn)_2Ni^{III}](ClO_4)_3$ (tacn =1,4,7-triazacyclononane), while the reaction of $[(talen^{t\text{-}Bu_2})Mn^{III}_3(solv)_n]^{3+}$ with $K_4[Os^{II}(CN)_6]$ and $NaClO_4{\cdot}H_2O$ yields $[\mathbf{Mn^{III}_6Os^{II}}](ClO_4)_2$ under an argon atmosphere. The molecular structure of $[\mathbf{Mn^{III}_6Os^{III}}]^{3+}$ as determined by single-crystal X-ray diffraction is closely related to the already published $[\mathbf{Mn^{III}_6M^c}]^{3+}$ complexes (M^c = Cr^{III}, Fe^{III}, Co^{III}, Mn^{III}). The half-wave potential of the Os^{III}/Os^{II} couple is $E_{1/2}$ = 0.07 V vs Fc^+/Fc. The FT-IR and electronic absorption spectra of $[\mathbf{Mn^{III}_6Os^{II}}]^{2+}$ and $[\mathbf{Mn^{III}_6Os^{III}}]^{3+}$ exhibit distinct features of dicationic and tricationic $[\mathbf{Mn^{III}_6M^c}]^{n+}$ complexes, respectively. The dc magnetic data (μ_{eff} vs T, M vs B, and VTVH) of $[\mathbf{Mn^{III}_6Os^{II}}]^{2+}$ are successfully simulated by a full-matrix diagonalization of a spin-Hamiltonian including isotropic exchange, zero-field splitting with full consideration of the relative orientation of the **D**-tensors, and Zeeman interaction, indicating antiferromagnetic Mn^{III}–Mn^{III} interactions within the trinuclear triplesalen subunits ($J^{(1)}_{Mn-Mn} = -(0.53 \pm 0.01)$ cm^{-1}, $\hat{H}_{ex} = -2\sum_{i<j} J_{ij}\hat{\mathbf{S}}_i{\cdot}\hat{\mathbf{S}}_j$) as well as across the central Os^{II} ion ($J^{(2,cis)}_{Mn-Mn} = -(0.06 \pm 0.01)$ cm^{-1}, $J^{(2,trans)}_{Mn-Mn} = -(0.15 \pm 0.01)$ cm^{-1}), while $D_{Mn} = -(3.9 \pm 0.1)$ cm^{-1}. The μ_{eff} vs T data of $[\mathbf{Mn^{III}_6Os^{III}}]^{3+}$ are excellently reproduced assuming an anisotropic Ising-like Os^{III}–Mn^{III} superexchange with a nonzero component $J^{(aniso)}_{Os-Mn} = -(11.0 \pm 1.0)$ cm^{-1} along the Os–Mn direction, while $J_{Mn-Mn} = -(0.9 \pm 0.1)$ cm^{-1} and $D_{Mn} = -(3.0 \pm 1.0)$ cm^{-1}. Alternating current measurements indicate a slower relaxation of the magnetization in the SMM $[\mathbf{Mn^{III}_6Os^{III}}]^{3+}$ compared to the 3d analogue $[\mathbf{Mn^{III}_6Fe^{III}}]^{3+}$ due to the stronger and anisotropic M^c–Mn^{III} exchange interaction.

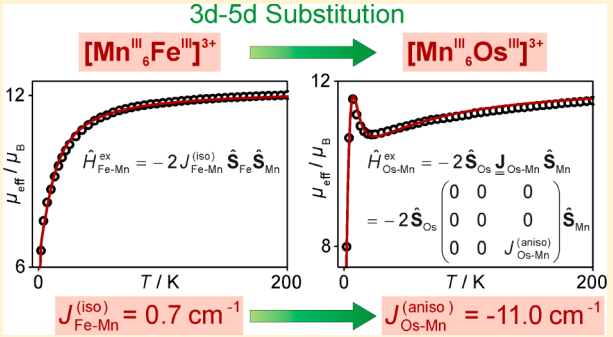

INTRODUCTION

Single-molecule magnet (SMM) behavior of coordination compounds has received a great deal of research attention since it was first reported in 1993.[1−10] The discovery of the archetype family of SMMs abbreviated $\mathbf{Mn_{12}}$ (= $[Mn^{III}_8Mn^{IV}_4O_{12}(O_2CR)_{16}(OH_2)_4]$)[1,2,11−20] was followed by many reports of SMM behavior for other 3d transition metal clusters.[21−32] In recent years, heavier transition metal ions[33−42] and lanthanide ions[43−58] have been increasingly targeted for incorporation into SMMs. A common feature of all SMMs is that they possess an energy barrier for magnetization reversal arising from the combination of a high total angular momentum ground state and strong magnetic anisotropy.[1,2,23,33,44,59−61]

We have developed a rational approach to SMMs based on a specifically designed ligand system.[62−66] Our SMMs are heptanuclear complexes $[\mathbf{M^t_6M^c}]^{n+}$ (= $[\{(talen^{t\text{-}Bu_2})M^t_3\}_2\{M^c(CN)_6\}]^{n+}$) formed by molecular recognition of two trinuclear complexes of a triplesalen ligand, $[(talen^{t\text{-}Bu_2})M^t_3]^{m+}$ (**A**, Scheme 1), with a hexacyanometalate (**B**).[67−71] The central phloroglucinol unit of the triplesalen ligand was chosen to promote high-spin ground states via the spin-polarization mechanism,[72−76] while the salen-like ligand compartments

Scheme 1. Trinuclear Triplesalen Complexes A and Their Assemblies with Hexacyanometalates B to Heptanuclear Complexes $[\mathbf{M^t_6M^c}]^{n+}$ by Molecular Recognition

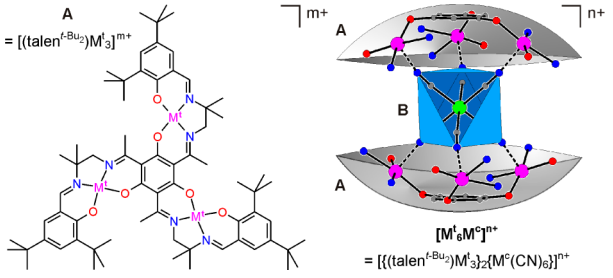

Received: August 29, 2013
Published: December 18, 2013

   dx.doi.org/10.1021/ic4022068 | Inorg. Chem. 2014, 53, 257−268

allow for single-site magnetic anisotropies through a strong tetragonal ligand field.[63,65,66,76,77] Our prototype SMM $[\mathbf{Mn^{III}_6Cr^{III}}]^{3+}$ possesses an energy barrier for magnetization reversal up to 28 K depending on the counterions and the solvent of crystallization,[67,68] while the SMM $[\mathbf{Mn^{III}_6Mn^{III}}]^{3+}$ exhibits a double hysteresis with hysteretic openings of the ground state and of an excited state up to 10 T.[69] In contrast, the $[\mathbf{Mn^{III}_6Fe^{III}}]^{3+}$ complex shows merely weak SMM behavior,[71] the reason for which has been elucidated through comparison with $[\mathbf{Mn^{III}_6Cr^{III}}]^{3+}$. While the J_{Cr-Mn} interaction is in the −4.0 to −5.0 cm^{-1} range for the $[\mathbf{Mn^{III}_6Cr^{III}}]^{3+}$ SMMs with the highest anisotropy barriers,[67,68] the J_{Fe-Mn} coupling in $[\mathbf{Mn^{III}_6Fe^{III}}]^{3+}$ is only +0.5 to +0.8 cm^{-1}.[71,78] Importantly, the J_{Cr-Mn} interaction is strong enough to overcome the weak antiferromagnetic J_{Mn-Mn} exchange in the trinuclear triplesalen subunits (−1.2 to −0.7 cm^{-1} in $[\mathbf{Mn^{III}_6Cr^{III}}]^{3+}$ and $[\mathbf{Mn^{III}_6Fe^{III}}]^{3+}$), which leads to a stabilized S_t = 21/2 spin ground state for $[\mathbf{Mn^{III}_6Cr^{III}}]^{3+}$, whereas the weak J_{Fe-Mn} interaction precludes the stabilization of a high-spin ground state and thus the development of an appreciable energy barrier for magnetization reversal in $[\mathbf{Mn^{III}_6Fe^{III}}]^{3+}$. This comparison illustrates the importance of a strong superexchange interaction via the $M^c-C\equiv N-Mn$ pathway for the manifestation of SMM behavior.

Taking these results into account, we have selected the $[Os^{III}(CN)_6]^{3-}$ building block (d^5 l.s., $^2T_{2g}$ ground state in O_h symmetry)[79] for incorporation into $[\mathbf{Mn^{III}_6M^c}]^{3+}$ based on the following rationales: (i) The increase in orbital extension when going from 3d to 4d and 5d transition metal ions generally promotes stronger superexchange interactions due to an increased orbital overlap with bridging ligands.[33] In this respect, a substantial strengthening of exchange couplings upon substitution of 3d ions with their 4d or 5d homologues has been confirmed by theory and experiment for $[M^{III}_2(CN)_{11}]^{5-}$ ($[\mathbf{M^{III}_2}]^{5-}$; M = Cr, Mo),[80,81] the linear complex $[\{Ni^{II}(cyclam)\}\{(Me_3tacn)M^{III}(CN)_3\}_2]^{2+}$ ($[\mathbf{Ni^{II}M^{III}_2}]^{2+}$; M = Cr, Mo; Me_3tacn = *N*,*N*′,*N*″-trimethyl-1,4,7-triazacyclononane, cyclam = 1,4,8,11-tetraazacyclotetradecane),[82,83] the trigonal-prismatic cluster $[Mn^{II}\{(Me_3tacn)M^{III}(CN)_3\}_6]^{2+}$ ($[\mathbf{Mn^{II}M^{III}_6}]^{2+}$; M = Cr, Mo),[34,83] and the star-like cluster $[\{V^{II}(PY5Me_2)\}_4\{M^{III}(CN)_6\}]^{5+}$ ($[\mathbf{V^{II}_4M^{III}}]^{5+}$; M = Cr, Mo; $PY5Me_2$ = 2,6-bis(1,1-bis(2-pyridyl)ethyl)pyridine),[84] as well as for the trigonal-bipyramidal compound $[\{Ni^{II}(tmphen)_2\}_3\{M^{III}(CN)_6\}_2]$ ($[\mathbf{Ni^{II}_2M^{III}_3}]$; M = Fe, Os; tmphen = 3,4,7,8-tetramethyl-1,10-phenanthroline)[85,86] and the linear complex $[\{Mn^{III}(5\text{-}Brsalen)(MeOH)\}_2\{M^{III}(CN)_6\}]^-$ ($[\mathbf{Mn^{III}_2M^{III}}]^-$; M = Fe, Ru, Os; 5-Brsalen = *N*,*N*′-ethylenebis-(5-bromosalicylideneiminato)).[40,41,87] (ii) Spin−orbit coupling is a relativistic effect, is much stronger for 4d and 5d transition metal ions than for 3d ions, and may thus promote stronger single-ion and/or exchange anisotropies. This has been shown for $[\mathbf{Ni^{II}M^{III}_2}]^{2+}$ and $[\mathbf{Mn^{II}M^{III}_6}]^{2+}$ (M = Cr, Mo) as well as for $[\mathbf{Ni^{II}_2M^{III}_3}]$ (M = Fe, Os) and $[\mathbf{Mn^{III}_2M^{III}}]^-$ (M = Fe, Ru, Os). In this respect, the $Os^{III}-Mn^{III}$ superexchange in $[\mathbf{Mn^{III}_2Os^{III}}]^-$ exhibits a strong three-axis anisotropy with $J_{xx} = -9$ cm^{-1}, $J_{yy} = +17.5$ cm^{-1}, and $J_{zz} = -16.5$ cm^{-1} ($\hat{H}^{eff}_{ex} = -2(J_{xx}\hat{\tau}_{Os,x}\hat{S}_{Mn,x} + J_{yy}\hat{\tau}_{Os,y}\hat{S}_{Mn,y} + J_{zz}\hat{\tau}_{Os,z}\hat{S}_{Mn,z})$ for the $Os^{III}-C\equiv N-Mn^{III}$ group with the pseudo-spin-1/2 operator $\hat{\tau}_{Os}$ for the Os^{III} ion and the true spin (S = 2) operator $\hat{S}_{Mn}$ for the Mn^{III} ion).[87] As a consequence of the substitution of the respective 3d ions with their 4d or 5d homologues, $[\mathbf{Mn^{II}Mo^{III}_6}]^{2+}$ shows SMM behavior in contrast to $[\mathbf{Mn^{II}Cr^{III}_6}]^{2+}$, while the series of $[\mathbf{Mn^{III}_2M^{III}}]^-$ SMMs exhibits higher energy barriers for magnetization reversal for M = Ru/Os compared to M = Fe.

In this contribution, we report the structural, spectroscopic, and magnetic properties of the SMM $[\mathbf{Mn^{III}_6Os^{III}}](ClO_4)_3$ and its one-electron-reduced congener $[\mathbf{Mn^{III}_6Os^{II}}](ClO_4)_2$. The comparison of the magnetic behavior of $[\mathbf{Mn^{III}_6Os^{III}}]^{3+}$ and $[\mathbf{Mn^{III}_6Fe^{III}}]^{3+}$[71,78] indicates that the substitution of the central Fe^{III} with its 5d homologue Os^{III} leads to a strengthening of the M^c-Mn^{III} exchange interaction along with the manifestation of exchange anisotropy resulting in an enhancement of SMM properties.

EXPERIMENTAL SECTION

Preparation of Compounds. $H_6talen^{t\text{-}Bu_2}$ {= 2,4,6-tris{1-[2-(3,5-di-*tert*-butylsalicylaldimino)-2-methylpropylimino]-ethyl}-1,3,5-trihydroxybenzene} was synthesized as described previously.[62,64] $K_4[Os^{II}(CN)_6]$,[88,89] $(Ph_4P)_3[Os^{III}(CN)_6]$,[79] and $[(tacn)_2Ni^{III}](ClO_4)_3$[90] were prepared as described in the literature. Filter paper for extremely fine precipitates was obtained from Machery-Nagel (grade no. 5, MN 619 de). Degassed solutions were prepared by three vacuum−argon cycles and handled under an argon atmosphere using the Schlenk technique.

CAUTION. *Perchlorate salts are potentially explosive and should only be prepared in small quantities and handled with appropriate precautions.*

$[\{(talen^{t\text{-}Bu_2})(Mn^{III}(MeOH))_3\}_2\{Os^{III}(CN)_6\}](ClO_4)_3\cdot 2.5MeOH$. A suspension of $H_6talen^{t\text{-}Bu_2}$ (297 mg, 0.267 mmol) and $Mn^{II}(OAc)_2\cdot 4H_2O$ (186 mg, 0.759 mmol) in methanol (100 mL) was heated at reflux for 2 h. The resulting brown solution was cooled to room temperature, purged with air for 30 min, and heated at reflux for additional 2 h. After cooling to room temperature the reaction solution was treated with a filtered solution of $(Ph_4P)_3[Os^{III}(CN)_6]$ (182 mg, 0.133 mmol) in methanol (6 mL). The reaction mixture was stirred at room temperature for 40 min and filtered. Addition of a solution of $NaClO_4\cdot H_2O$ (1902 mg, 13.54 mmol) in methanol (25 mL) to the filtrate resulted in the formation of a colorless precipitate, which was removed from the reaction mixture by filtration. Slow evaporation of the solvent from the filtrate afforded large brown rhombs, which were analyzed as $[\{(talen^{t\text{-}Bu_2})(Mn^{III}(MeOH))_3\}_2\{Os^{III}(CN)_6\}](ClO_4)_3\cdot 12MeOH$ by single-crystal X-ray diffraction and some small brown needles. The mixture of crystals (245 mg) was collected by filtration and resuspended in methanol (110 mL). The suspension was stirred at room temperature for 60 min and filtered. A solution of $[(tacn)_2Ni^{III}](ClO_4)_3$ (48 mg, 0.078 mmol) in acetonitrile (30 mL) was added to the filtrate. The resulting black solution was stirred at room temperature for 15 min and filtered. Slow evaporation of the solvent from the filtrate led to the deposition of a brown microcrystalline solid. Yield: 97 mg (22%). ESI-MS (MeCN): (+) *m*/*z* 962.9 $[\{(talen^{t\text{-}Bu_2})Mn_3\}_2\{Os(CN)_6\}]^{3+}$, 1443.8 $[\{(talen^{t\text{-}Bu_2})Mn_3\}_2\{Os(CN)_6\}]^{2+}$, 1452.2 $[\{(talen^{t\text{-}Bu_2})Mn_3\}_2\{Os(CN)_6\}(H_2O)]^{2+}$, 1460.7 $[\{(talen^{t\text{-}Bu_2})Mn_3\}_2\{Os(CN)_6\}(H_2O)_2]^{2+}$, 1493.2 $[\{(talen^{t\text{-}Bu_2})Mn_3\}_2\{Os(CN)_6\}(H_2O)_6]^{2+}$. MALDI-TOF-MS (matrix DCTB): (+) *m*/*z* 1443.4 $[\{(talen^{t\text{-}Bu_2})Mn_3\}_2\{Os(CN)_6\}]^{2+}$, 2886.5 $[\{(talen^{t\text{-}Bu_2})Mn_3\}_2\{Os(CN)_6\}]^{+}$, 2988.2 $\{[\{(talen^{t\text{-}Bu_2})Mn_3\}_2\{Os(CN)_6\}]ClO_4\}^{+}$, 3088.6 $\{[\{(talen^{t\text{-}Bu_2})Mn_3\}_2\{Os(CN)_6\}](ClO_4)_2\}^{+}$. IR: Nujol, $\tilde{\nu}$ (cm^{-1}) = 2112; KBr, $\tilde{\nu}$ (cm^{-1}) = 2959m, 2907m, 2868m, 2112m, 2058w, 2025w, 1611s, 1570s, 1535s, 1491vs, 1437m, 1395m, 1364m, 1341m, 1312m, 1275s, 1254s, 1190m, 1157m, 1144m, 1121s, 1109m, 1088m, 1026w, 847m, 820w, 781w, 750w, 644w, 625w, 608w, 577m, 552m. Anal. Found: C, 53.17; H, 6.25; N, 7.69. Calcd for $[\{(talen^{t\text{-}Bu_2})(Mn^{III}(MeOH))_3\}_2\{Os^{III}(CN)_6\}](ClO_4)_3\cdot 2.5MeOH$ ($C_{152.5}H_{226}N_{18}O_{32.5}Cl_3Mn_6Os$): C, 52.97; H, 6.59; N, 7.29.

$[\{(talen^{t\text{-}Bu_2})Mn^{III}\}_3]_2\{Os^{II}(CN)_6\}](ClO_4)_2\cdot 5MeOH\cdot 10H_2O$. A suspension of $H_6talen^{t\text{-}Bu_2}$ (221 mg, 0.199 mmol) and $Mn^{II}(OAc)_2\cdot 4H_2O$ (136 mg, 0.555 mmol) in methanol (80 mL) was heated at reflux for 2 h. The resulting brown solution was cooled to room temperature, purged with air for 30 min, and heated at reflux for additional 2 h. After cooling to room temperature the reaction solution was degassed and treated with a degassed solution of $K_4[Os^{II}(CN)_6]$ (51 mg, 0.10 mmol) and 18-

dx.doi.org/10.1021/ic4022068 | *Inorg. Chem.* 2014, 53, 257−268

crown-6 (787 mg, 2.98 mmol) in methanol (50 mL). The reaction mixture was stirred at room temperature for 40 min and filtered under an argon atmosphere. A degassed solution of $NaClO_4 \cdot H_2O$ (174 mg, 1.24 mmol) in methanol (24 mL) was added to the filtrate. The reaction solution was stirred at room temperature for 50 min and filtered under an argon atmosphere using. Slow evaporation of the solvent in a continuous argon flow over the filtrate afforded a brown solid. Yield: 232 mg (73%). ESI-MS (MeCN): (+) m/z 1443.6 $[\{(talen^{t\text{-}Bu_2})Mn_3\}_2\{Os(CN)_6\}]^{2+}$, 2886.9 $[\{(talen^{t\text{-}Bu_2})Mn_3\}_2\{Os(CN)_6\}]^{+}$, 2922.8 $[\{(talen^{t\text{-}Bu_2})Mn_3\}_2\{Os(CN)_6\}(H_2O)_2]^{+}$. MALDI-TOF-MS (matrix DCTB): (+) m/z 1443.2 $[\{(talen^{t\text{-}Bu_2})Mn_3\}_2\{Os(CN)_6\}]^{2+}$, 2886.7 $[\{(talen^{t\text{-}Bu_2})Mn_3\}_2\{Os(CN)_6\}]^{+}$, 2986.6 $\{[\{(talen^{t\text{-}Bu_2})Mn_3\}_2\{Os(CN)_6\}]ClO_4\}^{+}$, 3086.8 $\{[\{(talen^{t\text{-}Bu_2})Mn_3\}_2\{Os(CN)_6\}](ClO_4)_2\}^{+}$. IR: Nujol, $\tilde{\nu}$ (cm^{-1}) = 2058; KBr, $\tilde{\nu}$ (cm^{-1}) = 2957m, 2907m, 2870m, 2058vs, 2025w, 1613s, 1570s, 1535s, 1497s, 1437m, 1395m, 1364m, 1341m, 1308m, 1277s, 1254s, 1190m, 1152m, 1142m, 1121m, 1109m, 1065m, 1026w, 845m, 818w, 781w, 748w, 638w, 625w, 606w, 569m, 550s. Anal. Found: C, 51.95; H, 6.46; N, 7.52. Calcd for $[\{(talen^{t\text{-}Bu_2})Mn^{III}_3\}_2\{Os^{II}(CN)_6\}](ClO_4)_2 \cdot 5MeOH \cdot 10H_2O$ ($C_{149}H_{232}N_{18}O_{35}Cl_2Mn_6Os$): C, 52.23; H, 6.83; N, 7.36.

X-ray Crystallography. Brown single-crystals of $[\{(talen^{t\text{-}Bu_2})(Mn^{III}(MeOH))_3\}_2\{Os^{III}(CN)_6\}](ClO_4)_3 \cdot 12MeOH$ were removed from the mother liquor and immediately cooled to 100(2) K on a Bruker AXS Kappa ApexII diffractometer (four-circle goniometer with 4 K CCD detector, Mo Kα radiation, graphite monochromator). An empirical absorption correction using equivalent reflections was performed with the program SADABS 2008/1.[91] The structure was solved with the program SHELXS-97[92] and refined using SHELXL-97.[92] Crystal data and further details concerning the crystal structure determination are given in Table 1. CCDC 892630 contains the supplementary crystallographic data.

Table 1. Crystallographic Data for 1

empirical formula	$[C_{138}H_{192}N_{12}O_{12}Mn_6(CH_3OH)_6Os(CN)_6](ClO_4)_3 \cdot 12MeOH$
fw	3762.10
cryst syst	monoclinic
space group	$P2_1/n$
a (Å)	18.5295(11)
b (Å)	25.7151(15)
c (Å)	19.4977(10)
β (deg)	93.491(2)
V (Å^3)	9273.2(9)
Z	2
T (K)	100(2)
D_{calcd} (Mg/m^3)	1.347
μ(Mo Kα) (mm^{-1})	1.197
cryst size (mm)	0.26 × 0.25 × 0.20
θ range (deg)	2.44 to 27.00
reflns collected	451 544
indep reflns	20 212 (R(int) = 0.0232)
obsd reflns ($I > 2\sigma(I)$)	18 395
parameters	1166
goodness-of-fit on F^2	1.097
R_1/wR_2 ($I > 2\sigma(I)$)	0.0263/0.0643
max/min residuals (e × Å^{-3})	1.022/−0.883

Other Physical Measurements. Infrared spectra (400−4000 cm^{-1}) of solid samples were recorded on a Shimadzu FT-IR 8400S as KBr disks or as Nujol mulls on KBr disks. ESI and MALDI-TOF mass spectra were recorded on a Bruker Esquire 3000 ion trap mass spectrometer and a PE Biosystems Voyager DE mass spectrometer, respectively. Elemental analyses were carried out on a LECO CHN-932 or a HEKAtech Euro EA elemental analyzer. UV/vis/NIR absorption spectra of solutions were measured on a Shimadzu UV-3101PC spectrophotometer in the range 190−1200 nm at ambient temperatures. The electrochemical experiments were performed on Ar-flushed MeCN solutions containing 0.1 M $(NBu_4)PF_6$ in a classical three-electrode cell. The working electrode was a glassy carbon disk electrode, the counter electrode a platinum wire, and the reference electrode Ag/0.01 M $AgNO_3$ MeCN. All potentials are referenced to the ferrocenium/ferrocene (Fc^+/Fc) couple used as an internal standard. The electrochemical cell was connected to a Princeton Applied Research potentiostat/galvanostat model 263A. Temperature-dependent magnetic susceptibilities were measured using a SQUID magnetometer (MPMS XL-7 EC, Quantum Design) in a static field of 1 T in the range 2−290 K. Field-dependent magnetizations were measured at 2 K in the range 0.2−7 T. Variable-temperature variable-field (VTVH) measurements were performed at 1, 4, and 7 T in the range 2−10 K with the magnetization equidistantly sampled on a $1/T$ temperature scale. For calculations of the molar magnetic susceptibilities, χ_m, the measured susceptibilities were corrected for the underlying diamagnetism of the sample holder and the sample by using tabulated Pascal's constants. Alternating current susceptibilities were measured in the range 1.8−5.0 K in zero static field with an ac field of 3 Oe oscillating at frequencies in the range 660−1500 Hz.

Computational Details. The magnetic properties of $[\mathbf{Mn^{III}_6Os^{II}}]^{2+}$ and $[\mathbf{Mn^{III}_6Os^{III}}]^{3+}$ are simulated by a full-matrix diagonalization of the spin-Hamiltonian in eq 1.

$$\hat{H} = -2\sum_{i<j}\hat{\mathbf{S}}_i \cdot \underline{\underline{\mathbf{J}}}_{ij} \cdot \hat{\mathbf{S}}_j + \sum_i D_i(\hat{\mathbf{S}}_i \cdot \mathbf{e}_i(\vartheta_i, \varphi_i))^2 + \mu_B \sum_i \mathbf{B} \cdot \underline{\underline{\mathbf{g}}}_i \cdot \hat{\mathbf{S}}_i \quad (1)$$

Here the first sum reflects the exchange interaction between spins given by the spin vector operators $\hat{\mathbf{S}}_i$ at sites i. Exchange interactions between Mn^{III} ions are, as usual, supposed to be isotropic; that is, the tensor $\underline{\underline{\mathbf{J}}}_{ij}$ can be replaced by a scalar J_{ij}. In contrast, the exchange interactions of the Mn^{III} ions in $[\mathbf{Mn^{III}_6Os^{III}}]^{3+}$ with the Os^{III} ion, which is treated as a pseudo $S_i = 1/2$ spin,[40,87] are assumed to be anisotropic and thus modeled by a tensor.[87,93,94] The tensor is parametrized in the local coordinate system of the pair of interacting ions, where it is diagonal, as follows:

$$\underline{\underline{\mathbf{J}}}_{ij} = J^1_{ij}\mathbf{e}^1_{ij} \otimes \mathbf{e}^1_{ij} + J^2_{ij}\mathbf{e}^2_{ij} \otimes \mathbf{e}^2_{ij} + J^3_{ij}\mathbf{e}^3_{ij} \otimes \mathbf{e}^3_{ij} \quad (2)$$

In eq 2 the local unit vectors form an orthonormal system for which the 3-direction is chosen along the bond (exchange pathway) and the 1- and 2-directions are orthogonal. The unit vectors can be given by the respective angles in the global (molecular) coordinate system. "⊗" denotes the outer product. Due to the S_6 symmetry, all six exchange interactions between the Mn^{III} ions and the central Os^{III} are symmetry-related, which drastically reduces the number of unknown parameters.

The anisotropic magnetization behavior of the individual Mn^{III} ions is accounted for by local anisotropy tensors in the second sum. The tensors are approximated by their major axis and parametrized by a strength factor $D_i = D$ as well as local unit vectors $\mathbf{e}_i$, which are parametrized by polar angles ϑ_i and φ_i. They represent an easy or a hard axis depending on the sign of D. For the six Mn^{III} ions the unit vectors point along the local Jahn−Teller axes. Due to the S_6 symmetry all six local unit vectors $\mathbf{e}_i$ can be parametrized by the common polar angle between the Jahn−Teller axes and the S_6 symmetry axis, which has been extracted from the crystal structure of $[\mathbf{Mn^{III}_6Os^{III}}]^{3+}$ and is $\vartheta = 36.6°$. The relative φ_i angles are determined by the S_6 symmetry.

The third term of the Hamiltonian models the interaction with the applied magnetic field. $\underline{\underline{\mathbf{g}}}_i$ represents the local g-matrix at site i. For the Mn^{III} ions an isotropic $\underline{\underline{g}} = 1.98$ and for the Os^{III} ion in $[\mathbf{Mn^{III}_6Os^{III}}]^{3+}$ an isotropic $g = 1.8$ is assumed.[40,87] The Hilbert space of the full spin-Hamiltonian has a dimension of 15 625 for $[\mathbf{Mn^{III}_6Os^{II}}]^{2+}$ and 31 250 for $[\mathbf{Mn^{III}_6Os^{III}}]^{3+}$. In the presence of a magnetic field we employ inversion symmetry. This reduces the average matrix size to roughly half the full size. Since the measurements are performed on ensembles of small crystallites, we also employ an orientational average using an isotropic grid with 50 orientations.[78,95]

dx.doi.org/10.1021/ic4022068 | Inorg. Chem. 2014, 53, 257−268

RESULTS AND ANALYSIS

Synthesis and Characterization. $[Mn^{III}_6Os^{III}]^{3+}$ has been prepared in analogy to the synthesis of the heptanuclear triplesalen complexes $[Mn^{III}_6M^c]^{3+}$.[67−71,78,96] This resulted in single crystals, which were analyzed by single-crystal X-ray diffraction as $[\{(talen^{t\text{-}Bu_2})(Mn^{III}(MeOH))_3\}_2\{Os^{III}(CN)_6\}](ClO_4)_3\cdot 12MeOH$. However, the crystals were contaminated with a small amount of the reduced complex $[Mn^{III}_6Os^{II}](ClO_4)_2$ (see Supporting Information for further details), while some small needles were also found as a minor component, which were not suitable for single-crystal X-ray diffraction analysis. Pure batches of $[Mn^{III}_6Os^{III}](ClO_4)_3$ were obtained by recrystallization under an oxidizing atmosphere using $[(tacn)_2Ni^{III}](ClO_4)_3$ (tacn = 1,4,7-triazacyclononane).[90] Pure batches of $[Mn^{III}_6Os^{II}](ClO_4)_2$ were obtained using $[K(18\text{-crown-}6)]_4[Os^{II}(CN)_6]$ under an argon atmosphere (see Supporting Information for more details).

In addition to the differences relating to the ν(C≡N) vibrations (see Supporting Information), the FT-IR spectra of $[Mn^{III}_6Os^{III}]^{3+}$ and $[Mn^{III}_6Os^{II}]^{2+}$ exhibit some notable differences with respect to characteristic bands of the ligand $(talen^{t\text{-}Bu_2})^{6-}$. Interestingly, these differences seem to be universal for $[Mn^{III}_6M^c]^{3+}$ trications vs $[Mn^{III}_6M^c]^{2+}$ dications, as evident from comparison of the spectra of a series of $[Mn^{III}_6M^c]^{n+}$ complexes (M^c = Fe^{II}, Os^{II}, Mn^{III}, Cr^{III}, Co^{III}, Fe^{III}, Os^{III}) (Figure 1). The IR spectra of the tricationic

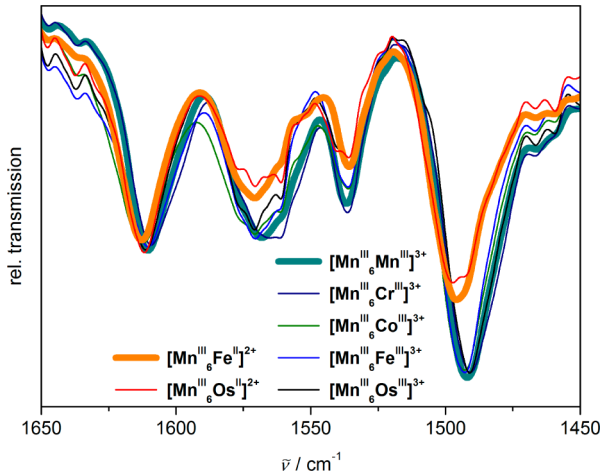

Figure 1. FT-IR spectra of various dicationic and tricationic $[Mn^{III}_6M^c]^{n+}$ complexes (M^c = Fe^{II},[71] Os^{II}, Mn^{III},[69,70] Cr^{III},[67,68] Co^{III},[96] Fe^{III},[71] Os^{III}) in KBr in the range 1650−1450 cm^{-1}.

$[Mn^{III}_6M^c]^{3+}$ complexes show prominent bands at 1611, 1570, 1535, and 1491 cm^{-1}, with the band at lowest energy being strongest in intensity. The respective region in the spectra of the $[Mn^{III}_6M^c]^{2+}$ dications also shows four bands. While virtually no change compared to the $[Mn^{III}_6M^c]^{3+}$ tricications is observed for the three bands at higher energy, the band at lowest energy shifts to 1497 cm^{-1} with a simultaneous decrease in intensity. Importantly, this band has been identified as a signature of the heteroradialene character of the central phloroglucinol backbone (*vide infra*) and most likely originates from vibrational modes with a pronounced C═O stretching character.[97,98]

Molecular and Crystal Structure. $[\{(talen^{t\text{-}Bu_2})(Mn^{III}(MeOH))_3\}_2\{Os^{III}(CN)_6\}](ClO_4)_3\cdot 12MeOH$ crystallizes in the space group $P2_1/n$. The asymmetric unit contains half of the $[Mn^{III}_6Os^{III}]^{3+}$ complex, with the other half being generated by a crystallographic center of inversion located at the central osmium ion. The $[Mn^{III}_6Os^{III}]^{3+}$ complex features two trinuclear Mn^{III} triplesalen subunits that are connected by $[Os^{III}(CN)_6]^{3-}$ (Figure 2). A thermal ellipsoid plot of the

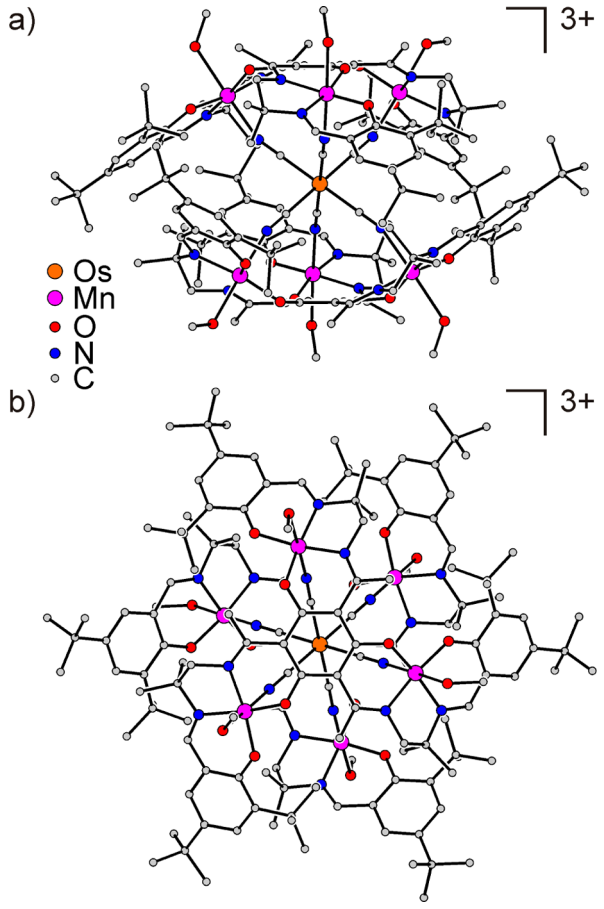

Figure 2. Molecular structure of $[\{(talen^{t\text{-}Bu_2})(Mn^{III}(MeOH))_3\}_2\{Os^{III}(CN)_6\}]^{3+}$ drawn (a) perpendicular and (b) parallel to the approximate molecular C_3 axis.

$[Mn^{III}_6Os^{III}]^{3+}$ fragment in the asymmetric unit is shown in Figure S1, and selected interatomic distances and angles are provided in Table S1 (Supporting Information). The $[Mn^{III}_6Os^{III}]^{3+}$ complexes include an angle of 70.6° between their approximate molecular C_3 axes. The distance between neighboring molecules as described by the shortest Os···Os distance is 18.31 Å, while the shortest intermolecular metal−metal distance of 8.47 Å is found between Mn^{III} ions. The Mn^{III} ions reside in a Jahn−Teller distorted tetragonal environment, with each Mn^{III} being coordinated by an N_2O_2 compartment of the ligand, with mean Mn−O^{Ph} and Mn−N^{imine} distances of 1.88 and 1.98 Å, respectively, and by a nitrogen atom of the $[Os^{III}(CN)_6]^{3-}$ unit (d(Mn−$N^{C\equiv N}$) = 2.19 Å) and the oxygen atom of a weakly coordinating methanol molecule (d(Mn−O^{MeOH}) = 2.34 Å). These distances are common for terminal Mn^{III} ions in $[Mn^{III}_6M^c]^{3+}$ carrying a methanol molecule at their sixth coordination site.[67−71,78,96]

The mean Os−C and C≡N bond lengths in $[\{(talen^{t\text{-}Bu_2})(Mn^{III}(MeOH))_3\}_2\{Os^{III}(CN)_6\}](ClO_4)_3\cdot 12MeOH$ are 2.05 and 1.15 Å, respectively, thus being identical to the respective mean values of 12 $Os(CN)_6$ fragments provided by a search in the Cambridge Structural Database (CSD). Only one of these

dx.doi.org/10.1021/ic4022068 | *Inorg. Chem.* 2014, 53, 257−268

fragments is part of an Os−C≡N−Mn unit, namely, that in $[\mathbf{Mn^{III}_2Os^{III}}]^-$.[40] This unit exhibits Os−C and C≡N bond distances of 2.05 and 1.16 Å, respectively, and a Mn−$N^{C\equiv N}$ bond length of 2.25 Å. The Os−C≡N units in $[\{(talen^{t\text{-}Bu_2})\text{-}(Mn^{III}(MeOH))_3\}_2\{Os^{III}(CN)_6\}](ClO_4)_3\cdot 12MeOH$ are almost linear with a mean angle of 178.8°, which is close to that of the 12 $Os(CN)_6$ fragments obtained from the CSD search (176.7°) and, in particular, to that of the Os−C≡N−Mn unit in $[\mathbf{Mn^{III}_2Os^{III}}]^-$ (176.2°). In contrast, the C≡N−Mn connections are bent with a mean angle of 160.2° in $[\{(talen^{t\text{-}Bu_2})\text{-}(Mn^{III}(MeOH))_3\}_2\{Os^{III}(CN)_6\}](ClO_4)_3\cdot 12MeOH$, which is significantly larger compared to $[\mathbf{Mn^{III}_2Os^{III}}]^-$ (143.3°), while it is common for our $[\mathbf{Mn^{III}_6M^c}]^{3+}$ complexes with various central metal ions.[67−71,78,96] Also, it is important to note that large spreads in the C≡N−Mn angle are generally observed for the $M(CN)_n$−C≡N−Mn unit irrespective of the cyanometalate.[68,70,78,100]

The bending of the C≡N−Mn units in $[\mathbf{Mn^{III}_6M^c}]^{3+}$ entails a symmetry reduction from approximately O_h to approximately C_3 with respect to the arrangement of the six terminal Mn^{III} ions around the central metal ion and affects the intramolecular Mn···Mn distances of $[\mathbf{Mn^{III}_6M^c}]^{3+}$, which are shorter for pairs of Mn^{III} ions of the same trinuclear triplesalen building block (~7 Å) than for pairs of Mn^{III} ions belonging to different trinuclear building blocks (~8 Å). A closer inspection of these Mn···Mn distances in conjunction with a detailed examination of other structural parameters in a series of $[\mathbf{Mn^{III}_6Fe^{III}}]^{3+}$,[78] $[\mathbf{Mn^{III}_6Co^{III}}]^{3+}$,[96] $[\mathbf{Mn^{III}_6Cr^{III}}]^{3+}$,[67,68] and $[\mathbf{Mn^{III}_6Mn^{III}}]^{3+}$[69,70] compounds has revealed that most $[\mathbf{Mn^{III}_6M^c}]^{3+}$ complexes belong to one of two types differing in (i) the topology of the $M^c(C\equiv N-Mn)_6$ unit as evidenced by the intramolecular Mn···Mn distances and the direction of the trigonal distortion of the $[M^c(CN)_6]^{3-}$ core and (ii) the kind of distortion of the salen subunits as described by two specific angles:

Type 1 exhibits intramolecular Mn···Mn distances in the 6.7−6.9 Å range for Mn^{III} ions belonging to the same trinuclear triplesalen building block and in the 7.8−8.2 Å range for Mn^{III} ions belonging to different trinuclear building blocks. The $[M^c(CN)_6]^{3-}$ core is slightly compressed along the approximate molecular C_3 axis, as evidenced by C−M^c−C angles > 90° within half of the complex. This type of $[\mathbf{Mn^{III}_6M^c}]^{3+}$ complexes is further characterized by a significant helical distortion of the salen subunits, which is reflected in a bent angle $\varphi^{central}$ = 180° − ∠(Mn−X_{NO}−X_R) (X_{NO}: midpoint of central adjacent N and O donor atoms; X_R: midpoint of the six-membered chelate ring containing the central N and O donor atoms)[101] in the 33−40° range and an angle $\theta^{central}$ = 7−13° between the central benzene plane and the vector defined by $O^{Ph}\cdots N^{ketimine}$ (Figure 3a).

Type 2 exhibits intramolecular Mn···Mn distances in the 6.6−6.8 Å and 8.0−8.4 Å ranges and a trigonally elongated $[M^c(CN)_6]^{3-}$ core (∠(C−M^c−C) < 90° within half of the complex), while $\varphi^{central}$ = 40−52° and $\theta^{central}$ = 0−5° (Figure 3b). These values for $\varphi^{central}$ and $\theta^{central}$ indicate a pronounced bending of the salen subunits along the $O^{Ph}\cdots N^{ketimine}$ vector rather than a helical distortion. Compared to type 1, the central phloroglucinol ring and its six direct substituents are more strongly distorted; that is, in type 2 the three oxygen atoms lie below and the three ketimine carbon atoms lie above the central benzene plane (Figure 3b), whereas in type 1 these six atoms and the phloroglucinol ring are in an idealized plane (Figure 3a).

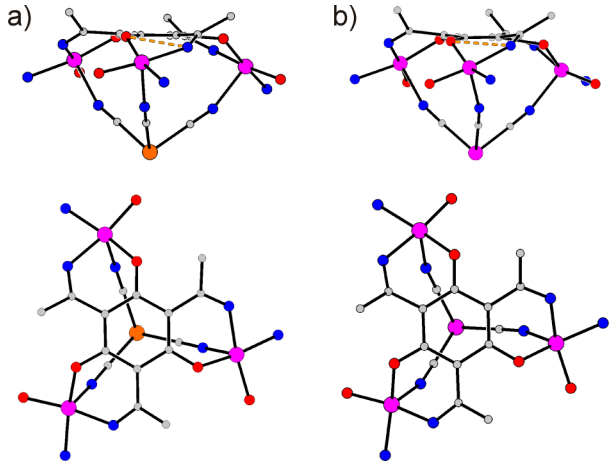

Figure 3. Sections of the molecular structures of (a) $[\mathbf{Mn^{III}_6Os^{III}}]^{3+}$ as a representative of type 1 $[\mathbf{Mn^{III}_6M^c}]^{3+}$ complexes and (b) a $[\mathbf{Mn^{III}_6Mn^{III}}]^{3+}$ complex[70] representing type 2, with the view direction in the benzene plane of the central phloroglucinol (top panels) and perpendicular to this plane (bottom panels). The dashed lines represent the vector defined by $O^{Ph}\cdots N^{ketimine}$ to visualize the angle $\theta^{central}$ between this vector and the central benzene plane.

The $[\mathbf{Mn^{III}_6Os^{III}}]^{3+}$ trication can be classified as a type 1 complex, as evidenced by (i) intramolecular Mn···Mn distances in the 6.81−6.89 Å range (mean value 6.85 Å) for Mn^{III} ions belonging to the same trinuclear triplesalen building block and in the 8.12−8.17 Å range (mean value 8.13 Å) for Mn^{III} ions belonging to different trinuclear building blocks; (ii) ∠(C−Os−C) = 90.2−91.6° (mean value 91.1°) within half of the complex; (iii) $\varphi^{central}$ = 33.0−38.5° (mean value 36.4°); and (iv) $\theta^{central}$ = 7.6−9.6° (mean value 8.4°).

The mean C−C and C−O bond lengths in the terminal phenolates of $[\mathbf{Mn^{III}_6Os^{III}}]^{3+}$ are 1.40 and 1.32 Å, respectively. In contrast, the central phloroglucinol ring exhibits a mean C−C bond length of 1.42 Å and a mean C−O bond length of 1.31 Å. The HOMA (harmonic oscillator model of aromaticity) index,[102−104] which is 1 for the model aromatic system benzene and 0 for the model nonaromatic system (benzene with localized double and single bonds), is 0.9 for the terminal phenol rings and 0.7 for the central ring. These distances and HOMA values are common for our tricationic $[\mathbf{Mn^{III}_6M^c}]^{3+}$ complexes,[68,70,71] indicating a significant keto-enamine (hetero-radialene) contribution to the resonance hybrid of the central phloroglucinol backbone.[98,105−107]

Electrochemistry. Cyclic and square-wave voltammograms of $[\mathbf{Mn^{III}_6Os^{III}}](ClO_4)_3$ have been recorded, and representative voltammograms are provided in Figure 4. The voltammograms exhibit a reversible redox wave with $E_{1/2}$ = 0.07 V (all potentials are referenced to the Fc^+/Fc couple). At higher potentials, several nonresolved redox events occur in the 0.7−1.4 V potential range. At negative potentials, the voltammograms exhibit a reversible reduction wave with $E_{1/2}$ = −0.76 V, followed by irreversible waves.

The voltammograms of $[\mathbf{Mn^{III}_6Os^{III}}]^{3+}$ closely resemble those of $[\mathbf{Mn^{III}_6Fe^{III}}]^{3+}$.[71] The reversible redox wave with $E_{1/2}$ = 0.07 V can be assigned to the Os^{III}/Os^{II} couple. Due to the higher tendency of a redox-active unit to be reduced with increasing positive charge,[108] the half-wave potential of the Os^{III}/Os^{II} couple is higher for $[\mathbf{Mn^{III}_6Os^{III}}]^{3+}$ than for $[Os^{III}(CN)_6]^{3-}$ ($E_{1/2}$ = −0.79 V in acetonitrile),[79] with the shift of approximately +0.9 V being common for our

dx.doi.org/10.1021/ic4022068 | Inorg. Chem. 2014, 53, 257−268

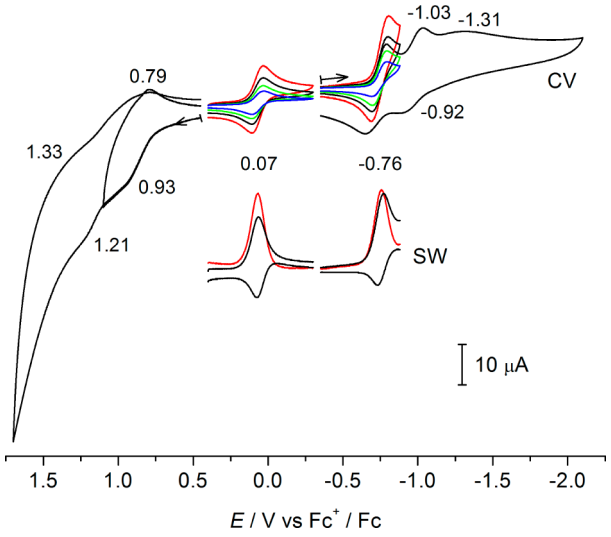

Figure 4. Cyclic (CV) and square-wave (SW) voltammograms of $[Mn^{III}_6Os^{III}](ClO_4)_3$ in MeCN solution (0.1 M $(NBu_4)PF_6$) at 20 °C recorded at a glassy carbon working electrode. CV: Scan rates 50 (blue), 100 (green), 200 (black), 400 (red) mV s^{-1}. SW: Frequency 60 Hz; I_f, I_r black, $I_f - I_r$ red.

$[Mn^{III}_6M^c]^{n+}$ complexes.[70,71] The irreversible redox waves at positive potentials originate from the Mn^{III} phenolate subunits, with the oxidations being most likely ligand-centered, leading to coordinated phenoxyl radicals,[64,65,97,105,109] while the redox waves at negative potentials arise from metal-centered redox events at the terminal Mn^{III} ions involving the Mn^{III}/Mn^{II} couple.[68,70,71]

Electronic Absorption Spectroscopy. The electronic absorption spectra of $[Mn^{III}_6Os^{III}](ClO_4)_3$ and $[Mn^{III}_6Os^{II}](ClO_4)_2$ dissolved in acetonitrile (Figure 5a) show strong features above 20000 cm^{-1} with a continuous increase in the absorption up to a maximum at 34 330 cm^{-1} (ε = 120 × 10^3 M^{-1} cm^{-1}) and 34 700 cm^{-1} (ε = 99 × 10^3 M^{-1} cm^{-1}), respectively. The spectrum of $(Ph_4P)_3[Os^{III}(CN)_6]$ in MeCN (Figure 5a) exhibits some very weak features below 35 000 cm^{-1} attributed to the $[Os^{III}(CN)_6]^{3-}$ anion, while the more intense transitions at higher energies mainly originate from the Ph_4P^+ counterions.[79,110] The colorless $K_4[Os^{II}(CN)_6]$ exhibits no transitions below 47 000 cm^{-1}.[110] On the other hand, the spectrum of the trinuclear triplesalen complex $[(talen^{t\text{-}Bu_2})\text{-}Mn^{III}_3(MeCN)_n]^{3+}$ shows strong transitions with an overall intensity of roughly 1/2 compared to the heptanuclear $[Mn^{III}_6Os^{III}]^{3+}$ and $[Mn^{III}_6Os^{II}]^{2+}$ complexes (Figure 5a).[100] These data indicate that, in analogy to the other $[Mn^{III}_6M^c]^{n+}$ complexes, the contribution of the hexacyanoosmate building block to the absorption spectra of $[Mn^{III}_6Os^{III}]^{3+}$ and $[Mn^{III}_6Os^{II}]^{2+}$ is negligible.

In a recent study comparing the absorption spectra of various $[Mn^{III}_6M^c]^{n+}$ complexes (M = Fe^{II}, Fe^{III}, Mn^{III}, Cr^{III}), we found that the spectrum of the $[Mn^{III}_6Fe^{II}]^{2+}$ dication differs considerably from the superimposable spectra of the $[Mn^{III}_6M^c]^{3+}$ trications.[71] This observation was related to structural differences in the Mn^{III}_3 triplesalen building block between $[Mn^{III}_6Fe^{II}]^{2+}$ and $[Mn^{III}_6M^c]^{3+}$, with the spectroscopic and structural data indicating a variation in the electronic structure of the central phloroglucinol backbone accompanying differences in the donor strengths of the Mn^{III} ligands.[71] The electronic absorption spectra of $[Mn^{III}_6Os^{II}]^{2+}$ and $[Mn^{III}_6Os^{III}]^{3+}$ suggest a generalization of this finding to

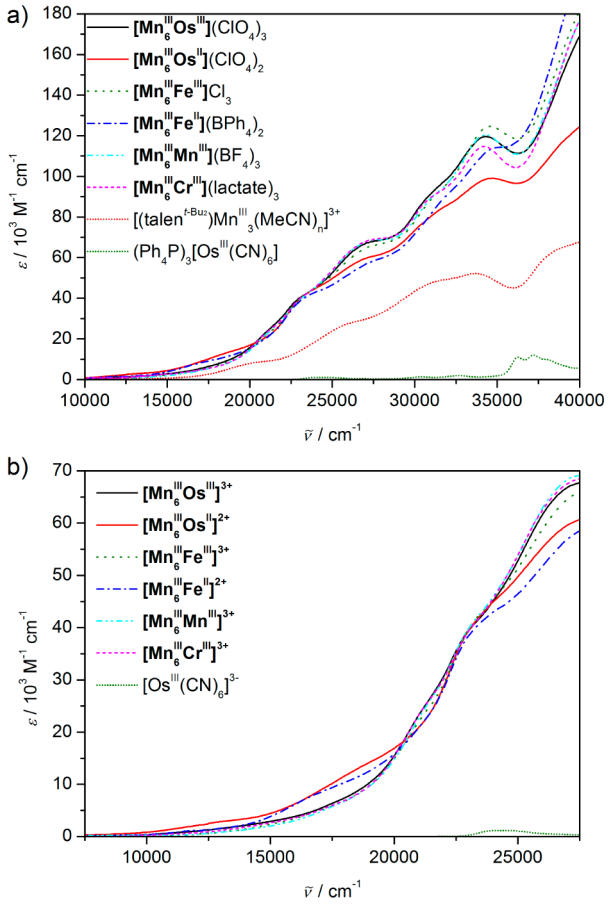

Figure 5. (a) Electronic absorption spectra of $[Mn^{III}_6Os^{III}](ClO_4)_3$, $[Mn^{III}_6Os^{II}](ClO_4)_2$, $[Mn^{III}_6Fe^{III}]Cl_3$,[71] $[Mn^{III}_6Fe^{II}](BPh_4)_2$,[71] $[Mn^{III}_6Mn^{III}](BF_4)_3$,[70] $[Mn^{III}_6Cr^{III}]$(lactate)$_3$,[68] $[(talen^{t\text{-}Bu_2})\text{-}Mn^{III}_3(MeCN)_n]^{3+}$ as generated *in situ*,[100] and $(Ph_4P)_3[Os^{III}(CN)_6]$, all measured in MeCN. (b) 7500−27500 cm^{-1} region of the electronic absorption spectra of $[Mn^{III}_6M^c]^{n+}$ (M^c = Os^{III}, Os^{II}, Fe^{III}, Fe^{II}, Mn^{III}, Cr^{III}) and $[Os^{III}(CN)_6]^{3-}$.

$[Mn^{III}_6M^c]^{2+}$ dications versus $[Mn^{III}_6M^c]^{3+}$ trications, as the spectrum of $[Mn^{III}_6Os^{II}]^{2+}$ resembles that of $[Mn^{III}_6Fe^{II}]^{2+}$ below 30 000 cm^{-1}, while the spectrum of $[Mn^{III}_6Os^{III}]^{3+}$ is virtually superimposable to the spectra of the other $[Mn^{III}_6M^c]^{3+}$ complexes (Figure 5).

We have quantified the differences in the ligand-field region (Figure 5b) by performing a Gaussian analysis on the spectra of $[Mn^{III}_6Os^{II}]^{2+}$ and $[Mn^{III}_6Os^{III}]^{3+}$. While using a locked background for the bands above 27 000 cm^{-1}, the fitting process for the region below 27 000 cm^{-1} was carried out with a minimum number of Gaussians for which the line-widths were correlated to the same value. In the case of $[Mn^{III}_6Os^{II}]^{2+}$, we achieved a good reproduction of the experimental data by incorporating four Gaussians (Table 2, Figure 6a), whereas for $[Mn^{III}_6Os^{III}]^{3+}$ (Figure 6b) only three Gaussians with a correlated line-width are resolved below 27 000 cm^{-1}, in analogy to $[Mn^{III}_6Cr^{III}]^{3+}$[68] and $[Mn^{III}_6Mn^{III}]^{3+}$.[70] Assuming C_{4v} symmetry of the coordination environment of the Mn^{III} ions in the trinuclear triplesalen building block in analogy to mononuclear Mn^{III} salen complexes,[111−117] three Mn^{III} ligand-field bands would be expected in the electronic absorption spectra of $[Mn^{III}_6M^c]^{n+}$, which can be assigned, from lower to higher energy, to the $^5B_1 \rightarrow {}^5A_1$, $^5B_1 \rightarrow {}^5B_2$, and $^5B_1 \rightarrow {}^5E$ transition.[68,118] However, the symmetry of the Mn^{III} environ-

dx.doi.org/10.1021/ic4022068 | Inorg. Chem. 2014, 53, 257−268

Table 2. Results of the Gaussian Analysis of the Electronic Absorption Spectra of $[Mn^{III}_6Os^{II}]^{2+}$ and $[Mn^{III}_6Os^{III}]^{3+}$ below 27 000 cm^{-1}

$[Mn^{III}_6Os^{II}]^{2+}$		$[Mn^{III}_6Os^{III}]^{3+}$	
$\tilde{\nu}_{max}/cm^{-1}$	$\varepsilon/10^3\ M^{-1}\ cm^{-1}$	$\tilde{\nu}_{max}/cm^{-1}$	$\varepsilon/10^3\ M^{-1}\ cm^{-1}$
12 800	2.3	13 600	1.7
16 700	5.1	17 600	5.2
19 700	12	21 400	18
23 800	40	[a]	[a]

[a]No further Gaussians with a correlated line-width are resolved.

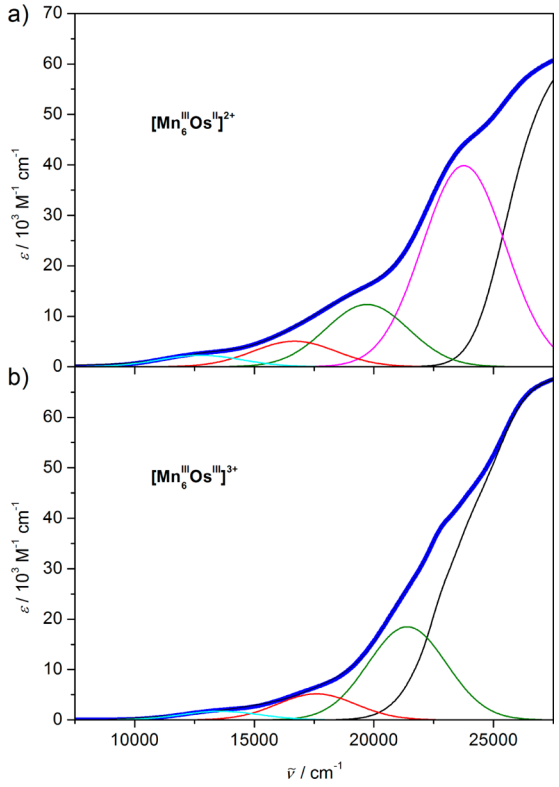

Figure 6. Gaussian resolution of the ligand-field region of the electronic absorption spectra of (a) $[Mn^{III}_6Os^{II}]^{2+}$ and (b) $[Mn^{III}_6Os^{III}]^{3+}$. The colored, thin lines represent the Gaussian peaks ascribed to ligand-field transitions. The black, thin line represents the sum of nonresolved Gaussian peaks at higher energies, the thick line the total sum, and the dashed line the experimental data.

ment in $[Mn^{III}_6M^c]^{n+}$ is lower than C_{4v}, which results in a removal of the degeneracy of the ^5E term and thus in the appearance of a fourth transition in the higher-energy region of the ligand-field spectra. This transition is resolved for $[Mn^{III}_6Os^{II}]^{2+}$, but not for $[Mn^{III}_6Os^{III}]^{3+}$ and the other tricationic $[Mn^{III}_6M^c]^{3+}$ complexes whose electronic absorption spectra were quantitatively analyzed.[68,70]

Comparison of transition energies for the two low-energy ligand-field transitions in $[Mn^{III}_6Os^{II}]^{2+}$ and $[Mn^{III}_6Os^{III}]^{3+}$ reveals a 800−900 cm^{-1} shift to higher energies with increasing oxidation state of the central metal ion, thus confirming our qualitative analysis of the ligand-field spectra of $[Mn^{III}_6Fe^{II}]^{2+}$ and $[Mn^{III}_6M^c]^{3+}$ (M = Fe^{III}, Mn^{III}, Cr^{III}).[71] The stronger ligand field in $[Mn^{III}_6M^c]^{3+}$ is a consequence of weaker π-donation to the Mn^{III} ions by the central oxygen atoms, which have more keto character in $[Mn^{III}_6M^c]^{3+}$ compared to $[Mn^{III}_6M^c]^{2+}$, and by the cyanide units, whose π^* orbitals experience less back-donation from $(M^c)^{III}$ compared to $(M^c)^{II}$.[71] This is corroborated by the lower heteroradialene transitions around 23 000 and 34 000 cm^{-1}.[68]

Magnetic Properties. Both complexes have been studied by dc (μ_{eff} vs T and VTVH[119]) and ac magnetic measurements. Alternating current magnetic measurements in zero dc field show a frequency-dependent onset of the out-of-phase component of the ac susceptibility at low temperatures for $[Mn^{III}_6Os^{III}]^{3+}$ (Figure 7), with a ratio $\chi'_M/\chi''_M = 0.93$ at 1488

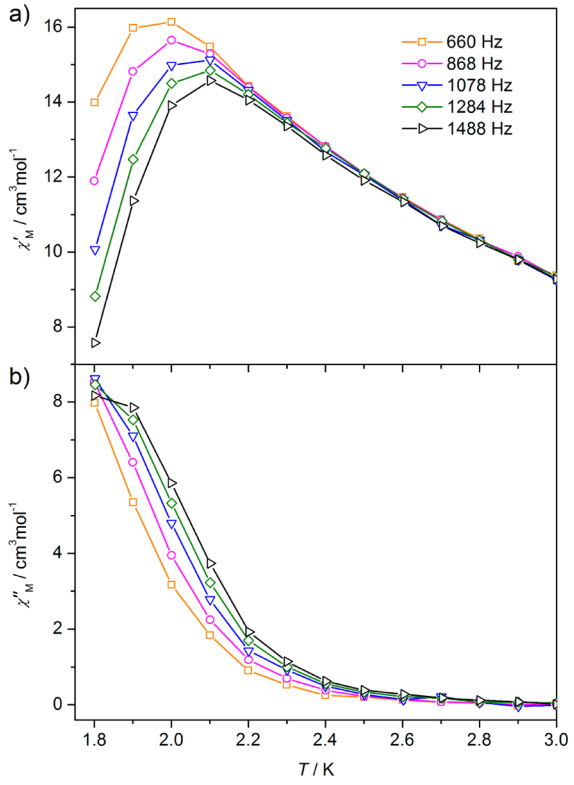

Figure 7. Plots of (a) the in-phase (χ'_M) and (b) the out-of-phase (χ''_M) component of the ac susceptibility versus the temperature for $[Mn^{III}_6Os^{III}](ClO_4)_3$ in zero dc field, with an ac field of 3 Oe oscillating at a frequency of 660 (orange), 868 (magenta), 1078 (blue), 1284 (green), and 1488 Hz (black). Solid lines are a guide to the eye.

Hz/1.8 K. The onset of χ''_M demonstrates a slow relaxation of the magnetization indicative of single-molecule magnet behavior. No onset of χ''_M is observed for $[Mn^{III}_6Os^{II}]^{2+}$.

$[Mn^{III}_6Os^{II}]^{2+}$. For the analysis of the magnetic data of $[Mn^{III}_6Os^{II}]^{2+}$, which possesses a diamagnetic central Os^{II} ion, first we used a coupling scheme with exchange interaction only between the Mn^{III} ions within each trinuclear triplesalen building block ($J^{(1)}_{Mn-Mn}$) (Figure 8a). This provided good

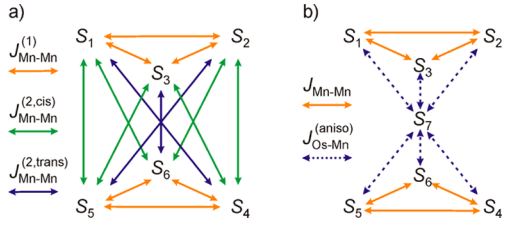

Figure 8. Coupling schemes for the analysis of the magnetic data of (a) $[Mn^{III}_6Os^{II}]^{2+}$ and (b) $[Mn^{III}_6Os^{III}]^{3+}$.

dx.doi.org/10.1021/ic4022068 | Inorg. Chem. 2014, 53, 257−268

reproductions for the μ_{eff} vs T curves but not for the VTVH measurements. Analogous behavior was already observed for $[\mathbf{Mn^{III}_6Co^{III}}]^{3+}$ and $[\mathbf{Mn^{III}_6Fe^{II}}]^{2+}$ also employing a diamagnetic central metal ion.[71,96] It was found that also an interaction across the central metal ion between Mn^{III} ions belonging to different trinuclear building blocks ($J^{(2)}_{Mn-Mn}$) had to be considered. Due to the S_6 symmetry, a coupling of an Mn^{III} ion in one trinuclear subunit with the Mn^{III} ions in *cis* position of the other subunit ($J^{(2,cis)}_{Mn-Mn}$) and the respective *trans* coupling ($J^{(2,trans)}_{Mn-Mn}$) were introduced (Figure 9a). For a detailed discussion, we refer to the references given.[71,96]

Simulations varying $J^{(1)}_{Mn-Mn}$, $J^{(2,cis)}_{Mn-Mn}$, $J^{(2,trans)}_{Mn-Mn}$, and D_{Mn} provided a parameter space that reproduced the magnetic data very well (Figure 9). From the variation of the simulations due to systematic changes in the parameters (only a few are provided in Figure 9), final parameters can be extracted: $J^{(1)}_{Mn-Mn} = -(0.53 \pm 0.01)$ cm^{-1}, $J^{(2,cis)}_{Mn-Mn} = -(0.06 \pm 0.01)$ cm^{-1}, $J^{(2,trans)}_{Mn-Mn} = -(0.15 \pm 0.01)$ cm^{-1}, and $D_{Mn} = -(3.9 \pm 0.1)$ cm^{-1}.

[Mn$^{III}_6$Os^{III}]$^{3+}$. In evaluating the magnetic properties of $[\mathbf{Mn^{III}_6Os^{III}}]^{3+}$, we have started with a minimum coupling scheme using isotropic coupling between the Mn^{III} ions belonging to one triplesalen subunit (J_{Mn-Mn}) and isotropic coupling between the Os^{III} ion and the Mn^{III} ions ($J^{(iso)}_{Os-Mn}$). The Os^{III} ion in $[Os^{III}(CN)_6]^{3-}$ (d^5 l.s., $^2T_{2g}$ ground state in O_h symmetry) experiences spin−orbit coupling of the effective $\tilde{L} = 1$ and the spin $S = 1/2$, resulting in a $\tilde{J} = 1/2$ ground state separated by ∼5000 cm^{-1} from a $\tilde{J} = 3/2$ excited multiplet.[40,79,86] Due to the large energy gap, the Os^{III} ion can thus be treated as a pseudo $S = 1/2$ spin.[40,86] Although the g tensor of the ground state of the Os^{III} ion may be anisotropic, we have assumed an isotropic effective g factor $g_{eff} = 1.8$ in analogy to the successful simulations of the magnetic data of the SMM $[\mathbf{Mn^{III}_2Os^{III}}]^-$.[40,87] Furthermore, we have taken into account a temperature-independent paramagnetism (TIP) contribution for the Os^{III} ion ($\chi_{TIP} = 2 \times 10^{-3}$ cm^3 mol^{-1}) in accordance with the results of theoretical and experimental studies on complexes of 5d ions with a $^2T_{2g}$ (O_h) ground state.[35,86,120]

With this coupling scheme, it was not possible to reproduce the minimum/sharp maximum feature in the μ_{eff} vs T data (see for example the green curve in Figure 10a). Therefore, we introduced an *anisotropic* exchange interaction between the central Os^{III} and each terminal Mn^{III} (Figure 8b). In order to gain a qualitative understanding of the impact of an anisotropic exchange between the central Os^{III} and each terminal Mn^{III}, and to avoid introducing an unjustifiably large number of parameters, we assumed an Ising-like exchange between the central Os^{III} and each terminal Mn^{III}. This means that $J^{(aniso)}_{Os-Mn}$ corresponds to J^3_{ij} in eq 2, whereas for the other two components $J^1_{ij} = J^2_{ij} = 0$ is assumed; that is, eq 2 becomes

$$\underline{\underline{\mathbf{J}}}_{ij} = J^{(aniso)}_{Os-Mn}\,\mathbf{e}^3_{ij} \otimes \mathbf{e}^3_{ij} \qquad (3)$$

For the direction $\mathbf{e}^3_{ij}$ of the Ising exchange we examined a few obvious candidates such as the Os−C$^{C\equiv N}$ direction, the global C_3-axis, and the direction of the local Jahn−Teller axes, which roughly correspond to the Os−Mn directions. Interestingly, the latter case yielded the best approximations for μ_{eff} vs T also perfectly matching the sharp maximum (Figure 10a). The simulations revealed a correlation between $J^{(aniso)}_{Os-Mn}$ and D_{Mn} (compare red and blue lines in Figure 10a). A reasonable parameter range with rather large variations for these parameters is provided by $J_{Mn-Mn} = -(0.9 \pm 0.1)$ cm^{-1}, $J^{(aniso)}_{Os-Mn} = -(11.0 \pm 1.0)$ cm^{-1}, and $D_{Mn} = -(3.0 \pm 1.0)$ cm^{-1}. It must be emphasized that the VTVH data at 4 and 7 T are only poorly reproduced by all simulations (Figure 10b). The restriction to an Ising-like anisotropic Os^{III}−Mn^{III} exchange has the advantage of providing only one parameter, but appears to be too simple to analyze the magnetic behavior of $[\mathbf{Mn^{III}_6Os^{III}}]^{3+}$, which likely exhibits a more complex Os^{III}−

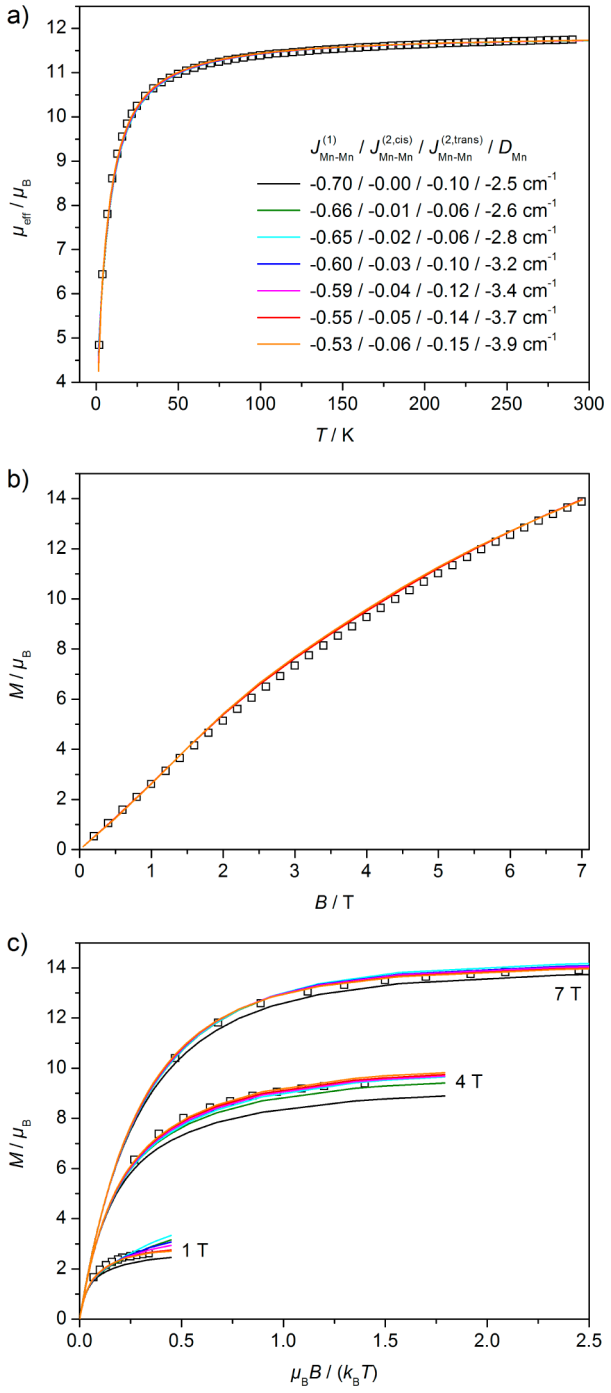

Figure 9. Simulations (lines) of (a) the μ_{eff} vs T data at 1 T, (b) the M vs B data at 2 K, and (c) the VTVH data at 1, 4, and 7 T of $[\mathbf{Mn^{III}_6Os^{II}}](ClO_4)_2$ performed by a full-matrix diagonalization of the spin-Hamiltonian in eq 1. Experimental data are given as symbols. The legend shown in (a) also applies to (b) and (c). The simulations (from black to orange) visualize the fitting of the VTVH data. Only the two best simulations (red and orange) are shown in (b).

dx.doi.org/10.1021/ic4022068 | Inorg. Chem. 2014, 53, 257−268

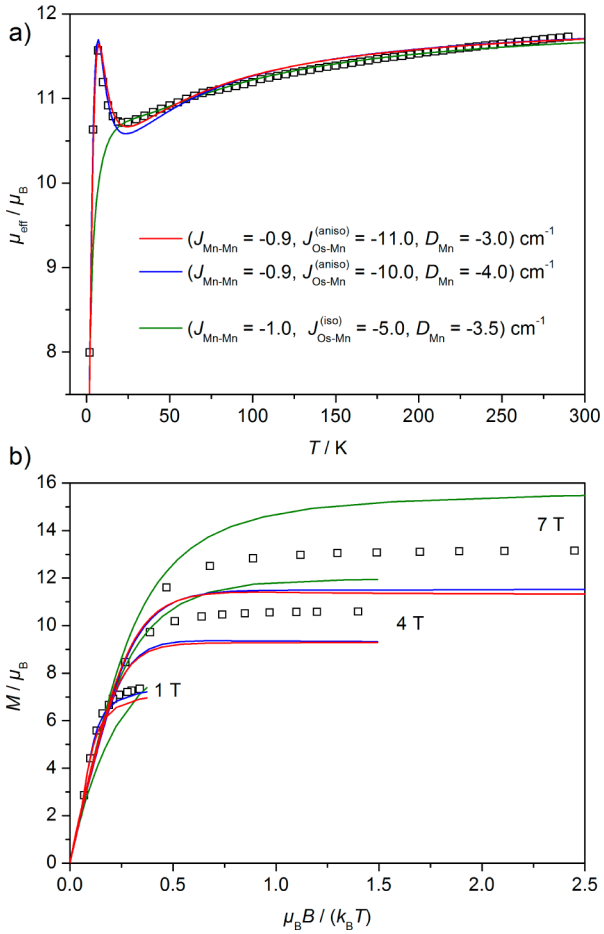

Figure 10. Simulations (lines) of (a) the μ_{eff} vs T data at 1 T and (b) the VTVH data at 1, 4, and 7 T of $[\mathbf{Mn^{III}_6Os^{III}}](ClO_4)_3$ performed by a full-matrix diagonalization of the spin-Hamiltonian in eq 1. The TIP-corrected experimental data are given as symbols. The legend shown in (a) also applies to (b).

Mn^{III} exchange anisotropy (that would require more parameters). This finding is in agreement with a recent study on the SMM $[\mathbf{Mn^{III}_2Os^{III}}]^{-}$.[87] Furthermore, the orientation of the Ising exchange has a strong influence on the VTVH simulation. The orientation along the Os−$C^{C\equiv N}$ direction appears to be more indicated, as it is the metal−ligand interaction in the exchange pathway and involves the covalent bond of the anisotropic Os^{III} ion. However, by forcing this direction, the anisotropic exchange tensor would have to contain more parameters. In light of the restricted experimental data and of the large dimension of the underlying Hilbert space, a complete evaluation of a parameter space with no restriction to the tensor directions and tensor elements is not feasible. Nevertheless, our simulations clearly demonstrate that the maximum of μ_{eff} at 10 K cannot be reproduced by an isotropic HDvV exchange Hamiltonian augmented with single-ion anisotropy, but unambiguously points to an anisotropic Os^{III}−Mn^{III} exchange interaction.

Finally, we would like to draw the reader's attention to an unusual phenomenon we encountered upon trying to simulate the magnetic data of $[\mathbf{Mn^{III}_6Os^{III}}]^{3+}$. As Figure 11 shows, the maximum of μ_{eff} at 10 K increases as D_{Mn} becomes more negative. Usually an increase in $|D|$ leads to a decrease of μ_{eff} at low temperatures for powder samples, which yield an average magnetic susceptibility to which the parallel susceptibility

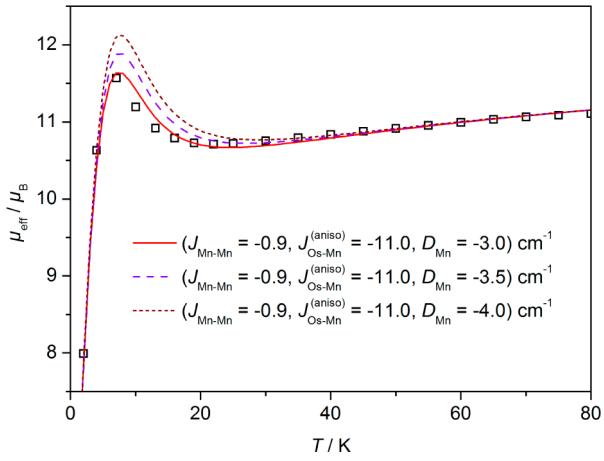

Figure 11. Simulations (lines) of the μ_{eff} vs T data at 1 T of $[\mathbf{Mn^{III}_6Os^{III}}](ClO_4)_3$ performed by a full-matrix diagonalization of the spin-Hamiltonian in eq 1. The TIP-corrected experimental data are shown as symbols. Note that the simulations illustrate a variation of D_{Mn}, while the other parameters remain constant.

(grows with increasing $|D|$ for $D < 0$) and the perpendicular susceptibility (decreases with increasing $|D|$ for $D < 0$) contribute approximately in the ratio 1:2.[119,121] Further investigations to elucidate the origin of the unusual behavior of μ_{eff} observed for our $[\mathbf{Mn^{III}_6Os^{III}}]^{3+}$ system are in progress.

DISCUSSION

Influence of the Oxidation State of the Central Metal Ion on the Structural and Electronic Properties of $[\mathbf{Mn^{III}_6M^c}]^{n+}$. The building block approach to our heptanuclear complexes of the $[\mathbf{M^t_6M^c}]^{n+}$ type has allowed the targeted replacement of the central $[Fe^{II/III}(CN)_6]^{4/3-}$ moiety in $[\mathbf{Mn^{III}_6Fe^{II/III}}]^{2/3+}$[71,78] with its 5d homologue $[Os^{II/III}(CN)_6]^{4/3-}$. Now two pairs of redox-related $[\mathbf{Mn^{III}_6M^c}]^{n+}$ complexes (M^c = Fe^{II}/Fe^{III},[71] Os^{II}/Os^{III}) have been investigated, which together with the various other tricationic $[\mathbf{Mn^{III}_6M^c}]^{3+}$ complexes (M^c = Cr^{III}, Co^{III}, Mn^{III}) allow generalizing some conclusions concerning the structural and electronic properties of the dicationic $[\mathbf{Mn^{III}_6M^c}]^{2+}$ complexes compared to the $[\mathbf{Mn^{III}_6M^c}]^{3+}$ trications.

The most striking evidence for a strong dependence of the electronic structure of the Mn^{III}_3 triplesalen subunits on the oxidation state (but not on the nature) of the central metal ion is provided by the infrared and electronic absorption spectra, which coincide for the two $[\mathbf{Mn^{III}_6M^c}]^{2+}$ dications as well as for all tricationic $[\mathbf{Mn^{III}_6M^c}]^{3+}$ complexes while differing substantially for the distinctly charged species. The observed differences are essentially related to the electronic structure of the central phloroglucinol backbone, whose resonance hybrid exhibits a stronger keto-enamine contribution in the tricationic complexes than in the dicationic ones. Importantly, the stronger phenolate character of the phloroglucinol unit (i.e., its higher degree of aromaticity) in $[\mathbf{Mn^{III}_6M^c}]^{2+}$ compared to $[\mathbf{Mn^{III}_6M^c}]^{3+}$ is reflected in the magnetic properties: there is a substantial weakening of the antiferromagnetic exchange interaction between the Mn^{III} ions in a trinuclear subunit with decreasing oxidation state of the central metal ion (from $[-1.2 \cdots -0.8]$ to -0.2 cm^{-1} for $[\mathbf{Mn^{III}_6Fe^{II/III}}]^{2/3+}$[71,78] and from -0.9 to -0.5 cm^{-1} for $[\mathbf{Mn^{III}_6Os^{II/III}}]^{2/3+}$). This weakening indicates a stronger ferromagnetic contribution to

dx.doi.org/10.1021/ic4022068 | Inorg. Chem. 2014, 53, 257−268

the Mn^{III}−Mn^{III} exchange interaction due to a greater efficiency of the spin-polarization mechanism.

Influence of 3d−5d Transition Metal Substitution on the SMM Properties of $[Mn^{III}_6M^c]^{3+}$. The $[Mn^{III}_6Os^{III}]^{3+}$ complex is the first $[M^t_6M^c]^{n+}$-type SMM incorporating a 5d transition metal ion. The strong spin−orbit coupling in the 5d ion Os^{III}, which exhibits an orbitally degenerate ground state, results in orbitally dependent and highly anisotropic exchange interactions.[42,93,122−125] In this respect, simulations of the magnetic data of the SMMs $[Mn^{III}_2Os^{III}]^{-}$[40,87] and $[Mn^{III}_2Ru^{III}]^{-}$[41,87] as well as of the $[Ni^{II}_2Os^{III}_3]$ complex[86,93] revealed strong exchange anisotropy.

We thus modified our spin-Hamiltonian to account for an anisotropic Os^{III}−Mn^{III} superexchange and achieved an excellent reproduction of the μ_{eff} vs T data of $[Mn^{III}_6Os^{III}]^{3+}$ within this model. This indicates that in $[Mn^{III}_6Os^{III}]^{3+}$ not only the single-ion anisotropies of the Mn^{III} ions contribute to the magnetic anisotropy of the ground state—and thus to the energy barrier for magnetization reversal—but also the superexchange interactions. Furthermore, the magnitude of the Os^{III}−Mn^{III} interaction ($J^{(aniso)}_{Os-Mn}$ = −11.0 cm^{-1}) demonstrates a substantial strengthening compared to $[Mn^{III}_6Fe^{III}]^{3+}$ (J_{Fe-Mn} = +0.5 to +0.8 cm^{-1}).[71,78] The resulting enhanced stabilization of the ground state in $[Mn^{III}_6Os^{III}]^{3+}$ compared to $[Mn^{III}_6Fe^{III}]^{3+}$ is reflected in the μ_{eff} vs T curves of the two compounds, with $[Mn^{III}_6Os^{III}]^{3+}$ exhibiting an increase in μ_{eff} at low temperatures in contrast to $[Mn^{III}_6Fe^{III}]^{3+}$, for which μ_{eff} steadily decreases with decreasing temperature.

Overall, the enhancement of the M^c−Mn^{III} interaction together with the manifestation of exchange anisotropy, which both originate from the replacement of the 3d ion Fe^{III} with its 5d homologue Os^{III}, leads to a slower relaxation of the magnetization in $[Mn^{III}_6Os^{III}]^{3+}$ compared to $[Mn^{III}_6Fe^{III}]^{3+}$. This can be inferred from ac measurements showing a stronger splitting of χ'_M for various frequencies for $[Mn^{III}_6Os^{III}]^{3+}$ and a ratio χ'_M/χ''_M = 0.93 at 1488 Hz/1.8 K, which is 3.97 in $[Mn^{III}_6Fe^{III}]^{3+}$.

■ ASSOCIATED CONTENT

Supporting Information

Details of synthesis and characterization. Crystallographic file in CIF format, thermal ellipsoid plot, and selected bond distances and angles for $[Mn^{III}_6Os^{III}](ClO_4)_3$. This material is available free of charge via the Internet at http://pubs.acs.org.

■ AUTHOR INFORMATION

Corresponding Authors

*E-mail: jschnack@uni-bielefeld.de.

*E-mail: thorsten.glaser@uni-bielefeld.de.

Notes

The authors declare no competing financial interest.

■ ACKNOWLEDGMENTS

We thank the Fonds der Chemischen Industrie, the DFG (FOR945 "Nanomagnets"), and Bielefeld University for financial support. V.H. also gratefully acknowledges the Fonds der Chemischen Industrie for a doctoral fellowship.

■ REFERENCES

(1) Sessoli, R.; Gatteschi, D.; Caneschi, A.; Novak, M. A. *Nature* **1993**, *365*, 141−143.

(2) Sessoli, R.; Tsai, H. L.; Schake, A. R.; Wang, S. Y.; Vincent, J. B.; Folting, K.; Gatteschi, D.; Christou, G.; Hendrickson, D. N. *J. Am. Chem. Soc.* **1993**, *115*, 1804−1816.

(3) Dei, A.; Gatteschi, D. *Angew. Chem., Int. Ed.* **2011**, *50*, 11852−11858.

(4) Tejada, J. *Polyhedron* **2001**, *20*, 1751−1756.

(5) Tejada, J.; Chudnovsky, E. M.; del Barco, E.; Hernandez, J. M.; Spiller, T. P. *Nanotechnology* **2001**, *12*, 181−186.

(6) Awschalom, D. D.; Di Vincenzo, D. P.; Smyth, J. J. *Science* **1992**, *258*, 414−421.

(7) Leuenberger, M. N.; Loss, D. *Nature* **2001**, *410*, 789−793.

(8) Cornia, A.; Fabretti, A. C.; Pacchioni, M.; Zobbi, L.; Bonacchi, D.; Caneschi, A.; Gatteschi, D.; Biagi, R.; Del Pennino, U.; De Renzi, V.; Gurevich, L.; Van der Zant, H. S. J. *Angew. Chem., Int. Ed.* **2003**, *42*, 1645−1648.

(9) Bogani, L.; Wernsdorfer, W. *Nat. Mater.* **2008**, *7*, 179−186.

(10) Chiesa, A.; Carretta, S.; Santini, P.; Amoretti, G.; Pavarini, E. *Phys. Rev. Lett.* **2013**, *110*, 157204.

(11) Bagai, R.; Christou, G. *Chem. Soc. Rev.* **2009**, *38*, 1011−1026.

(12) Wernsdorfer, W.; Sessoli, R.; Gatteschi, D. *Europhys. Lett.* **1999**, *47*, 254−259.

(13) Aubin, S. M. J.; Sun, Z.; Eppley, H. J.; Rumberger, E. M.; Guzei, I. A.; Folting, K.; Gantzel, P. K.; Rheingold, A. L.; Christou, G.; Hendrickson, D. N. *Inorg. Chem.* **2001**, *40*, 2127−2146.

(14) Boskovic, C.; Pink, M.; Huffman, J. C.; Hendrickson, D. N.; Christou, G. *J. Am. Chem. Soc.* **2001**, *123*, 9914−9915.

(15) Mertes, K. M.; Suzuki, Y.; Sarachik, M. P.; Paltiel, Y.; Shtrikman, H.; Zeldov, E.; Rumberger, E.; Hendrickson, D. N.; Christou, G. *Phys. Rev. Lett.* **2001**, *87*, 227205.

(16) Cornia, A.; Sessoli, R.; Sorace, L.; Gatteschi, D.; Barra, A. L.; Daiguebonne, C. *Phys. Rev. Lett.* **2002**, *89*, 257201.

(17) Sòler, M.; Wernsdorfer, W.; Abboud, K. A.; Huffman, J. C.; Davidson, E. R.; Hendrickson, D. N.; Christou, G. *J. Am. Chem. Soc.* **2003**, *125*, 3576−3588.

(18) Chakov, N. E.; Soler, M.; Wernsdorfer, W.; Abboud, K. A.; Christou, G. *Inorg. Chem.* **2005**, *44*, 5304−5321.

(19) Wernsdorfer, W.; Murugesu, M.; Christou, G. *Phys. Rev. Lett.* **2006**, *96*, 057208.

(20) Hill, S.; Murugesu, M.; Christou, G. *Phys. Rev. B* **2009**, *80*, 174416.

(21) Winpenny, R. E. P. *J. Chem. Soc., Dalton Trans.* **2002**, 1−10.

(22) Aromi, G.; Brechin, E. K. *Struct. Bonding (Berlin)* **2006**, *122*, 1−67.

(23) Gatteschi, D.; Sessoli, R.; Villain, J. *Molecular Nanomagnets*; Oxford University Press: Oxford, 2006.

(24) Miyasaka, H.; Saitoh, A.; Abe, S. *Coord. Chem. Rev.* **2007**, *251*, 2622−2664.

(25) Roubeau, O.; Clérac, R. *Eur. J. Inorg. Chem.* **2008**, 4325−4342.

(26) Kostakis, G. E.; Ako, A. M.; Powell, A. K. *Chem. Soc. Rev.* **2010**, *39*, 2238−2271.

(27) Murrie, M. *Chem. Soc. Rev.* **2010**, *39*, 1986−1995.

(28) Beltran, L. M. C.; Long, J. R. *Acc. Chem. Res.* **2005**, *38*, 325−334.

(29) Rebilly, J.-N.; Mallah, T. *Struct. Bonding (Berlin)* **2006**, *122*, 103−131.

(30) Atanasov, M.; Comba, P.; Hausberg, S.; Martin, B. *Coord. Chem. Rev.* **2009**, *253*, 2306−2314.

(31) Das, A.; Gieb, K.; Krupskaya, Y.; Demeshko, S.; Dechert, S.; Klingeler, R.; Kataev, V.; Büchner, B.; Müller, P.; Meyer, F. *J. Am. Chem. Soc.* **2011**, *133*, 3433−3443.

(32) Garlatti, E.; Carretta, S.; Santini, P.; Amoretti, G.; Mariani, M.; Lascialfari, A.; Sanna, S.; Mason, K.; Chang, J.; Tasker, P.; Brechin, E. K. *Phys. Rev. B* **2013**, *87*, 054409.

(33) Wang, X.-Y.; Avendaño, C.; Dunbar, K. R. *Chem. Soc. Rev.* **2011**, *40*, 3213−3238.

(34) Sokol, J. J.; Hee, A. G.; Long, J. R. *J. Am. Chem. Soc.* **2002**, *124*, 7656−7657.

(35) Schelter, E. J.; Prosvirin, A. V.; Dunbar, K. R. *J. Am. Chem. Soc.* **2004**, *126*, 15004−15005.

(36) Martínez-Lillo, J.; Armentano, D.; De Munno, G.; Wernsdorfer, W.; Julve, M.; Lloret, F.; Faus, J. *J. Am. Chem. Soc.* **2006**, *128*, 14218−14219.
(37) Freedman, D. E.; Jenkins, D. M.; Iavarone, A. T.; Long, J. R. *J. Am. Chem. Soc.* **2008**, *130*, 2884−2885.
(38) Hilfiger, M. G.; Zhao, H.; Prosvirin, A.; Wernsdorfer, W.; Dunbar, K. R. *Dalton Trans.* **2009**, 5155−5163.
(39) Zadrozny, J. M.; Freedman, D. E.; Jenkins, D. M.; Harris, T. D.; Iavarone, A. T.; Mathonière, C.; Clérac, R.; Long, J. R. *Inorg. Chem.* **2010**, *49*, 8886−8896.
(40) Pedersen, K. S.; Schau-Magnussen, M.; Bendix, J.; Weihe, H.; Palii, A. V.; Klokishner, S. I.; Ostrovsky, S.; Reu, O. S.; Mutka, H.; Tregenna-Piggott, P. L. W. *Chem.—Eur. J.* **2010**, *16*, 13458−13464.
(41) Pedersen, K. S.; Dreiser, J.; Nehrkorn, J.; Gysler, M.; Schau-Magnussen, M.; Schnegg, A.; Holldack, K.; Bittl, R.; Piligkos, S.; Weihe, H.; Tregenna-Piggott, P.; Waldmann, O.; Bendix, J. *Chem. Commun.* **2011**, *47*, 6918−6920.
(42) Mironov, V. S.; Chibotaru, L. F.; Ceulemans, A. *J. Am. Chem. Soc.* **2003**, *125*, 9750−9760.
(43) Sorace, L.; Benelli, C.; Gatteschi, D. *Chem. Soc. Rev.* **2011**, *40*, 3092−3104.
(44) Rinehart, J. D.; Long, J. R. *Chem. Sci.* **2011**, *2*, 2078−2085.
(45) Sessoli, R.; Powell, A. *Coord. Chem. Rev.* **2009**, *253*, 2328−2341.
(46) Katoh, K.; Isshiki, H.; Komeda, T.; Yamashita, M. *Coord. Chem. Rev.* **2011**, *255*, 2124−2148.
(47) Ishikawa, N.; Sugita, M.; Ishikawa, T.; Koshihara, S.; Kaizu, Y. *J. Am. Chem. Soc.* **2003**, *125*, 8694−8695.
(48) Gonidec, M.; Luis, F.; Vílchez, À.; Esquena, J.; Amabilino, D. B.; Veciana, J. *Angew. Chem., Int. Ed.* **2010**, *49*, 1623−1626.
(49) Guo, Y.-N.; Xu, G.-F.; Wernsdorfer, W.; Ungur, L.; Guo, Y.; Tang, J.; Zhang, H.-J.; Chibotaru, L. F.; Powell, A. K. *J. Am. Chem. Soc.* **2011**, *133*, 11948−11951.
(50) Hewitt, I. J.; Tang, J.; Madhu, N. T.; Anson, C. E.; Lan, Y.; Luzon, J.; Etienne, M.; Sessoli, R.; Powell, A. K. *Angew. Chem., Int. Ed.* **2010**, *49*, 6352−6356.
(51) Rinehart, J. D.; Fang, M.; Evans, W. J.; Long, J. R. *Nat. Chem.* **2011**, *3*, 538−542.
(52) Rinehart, J. D.; Fang, M.; Evans, W. J.; Long, J. R. *J. Am. Chem. Soc.* **2011**, *133*, 14236−14239.
(53) Ako, A. M.; Mereacre, V.; Clérac, R.; Wernsdorfer, W.; Hewitt, I. J.; Anson, C. E.; Powell, A. K. *Chem. Commun.* **2009**, 544−546.
(54) Karotsis, G.; Kennedy, S.; Teat, S. J.; Beavers, C. M.; Fowler, D. A.; Morales, J. J.; Evangelisti, M.; Dalgarno, S. J.; Brechin, E. K. *J. Am. Chem. Soc.* **2010**, *132*, 12983−12990.
(55) Habib, F.; Murugesu, M. *Chem. Soc. Rev.* **2013**, *42*, 3278−3288.
(56) Le Roy, J. J.; Jeletic, M.; Gorelsky, S. I.; Korobkov, I.; Ungur, L.; Chibotaru, L. F.; Murugesu, M. *J. Am. Chem. Soc.* **2013**, *135*, 3502−3510.
(57) Blagg, R. J.; Ungur, L.; Tuna, F.; Speak, J.; Comar, P.; Collison, D.; Wernsdorfer, W.; McInnes, E. J. L.; Chibotaru, L. F.; Winpenny, R. E. P. *Nat. Chem.* **2013**, *5*, 673−678.
(58) Woodruff, D. N.; Winpenny, R. E. P.; Layfield, R. A. *Chem. Rev.* **2013**, *113*, 5110−5148.
(59) Gatteschi, D.; Sessoli, R. *Angew. Chem., Int. Ed.* **2003**, *42*, 268−297.
(60) Christou, G.; Gatteschi, D.; Hendrickson, D. N.; Sessoli, R. *MRS Bull.* **2000**, *25*, 66−71.
(61) Thomas, L.; Lionti, F.; Ballou, R.; Gatteschi, D.; Sessoli, R.; Barbara, B. *Nature* **1996**, *383*, 145−147.
(62) Glaser, T.; Heidemeier, M.; Lügger, T. *Dalton Trans.* **2003**, 2381−2383.
(63) Glaser, T.; Heidemeier, M.; Grimme, S.; Bill, E. *Inorg. Chem.* **2004**, *43*, 5192−5194.
(64) Glaser, T.; Heidemeier, M.; Fröhlich, R.; Hildebrandt, P.; Bothe, E.; Bill, E. *Inorg. Chem.* **2005**, *44*, 5467−5482.
(65) Glaser, T.; Heidemeier, M.; Strautmann, J. B. H.; Bögge, H.; Stammler, A.; Krickemeyer, E.; Huenerbein, R.; Grimme, S.; Bothe, E.; Bill, E. *Chem.—Eur. J.* **2007**, *13*, 9191−9206.
(66) Theil, H.; Freiherr von Richthofen, C.-G.; Stammler, A.; Bögge, H.; Glaser, T. *Inorg. Chim. Acta* **2008**, *361*, 916−924.
(67) Glaser, T.; Heidemeier, M.; Weyhermüller, T.; Hoffmann, R.-D.; Rupp, H.; Müller, P. *Angew. Chem., Int. Ed.* **2006**, *45*, 6033−6037.
(68) Hoeke, V.; Heidemeier, M.; Krickemeyer, E.; Stammler, A.; Bögge, H.; Schnack, J.; Postnikov, A.; Glaser, T. *Inorg. Chem.* **2012**, *51*, 10929−10954.
(69) Hoeke, V.; Gieb, K.; Müller, P.; Ungur, L.; Chibotaru, L. F.; Heidemeier, M.; Krickemeyer, E.; Stammler, A.; Bögge, H.; Schröder, C.; Schnack, J.; Glaser, T. *Chem. Sci.* **2012**, *3*, 2868−2882.
(70) Hoeke, V.; Heidemeier, M.; Krickemeyer, E.; Stammler, A.; Bögge, H.; Schnack, J.; Glaser, T. *Dalton Trans.* **2012**, *41*, 12942−12959.
(71) Hoeke, V.; Krickemeyer, E.; Heidemeier, M.; Theil, H.; Stammler, A.; Bögge, H.; Weyhermüller, T.; Schnack, J.; Glaser, T. *Eur. J. Inorg. Chem.* **2013**, 4398−4409.
(72) Longuet-Higgins, H. C. *J. Chem. Phys.* **1950**, *18*, 265−274.
(73) McConnell, H. M. *J. Chem. Phys.* **1963**, *39*, 1910.
(74) Fernández, I.; Ruiz, R.; Faus, J.; Julve, M.; Lloret, F.; Cano, J.; Ottenwaelder, X.; Journaux, Y.; Munoz, C. *Angew. Chem., Int. Ed.* **2001**, *40*, 3039−3042.
(75) Pardo, E.; Ruiz-Garcia, R.; Cano, J.; Ottenwaelder, X.; Lescouezec, R.; Journaux, Y.; Lloret, F.; Julve, M. *Dalton Trans.* **2008**, 2780−2805.
(76) Glaser, T.; Gerenkamp, M.; Fröhlich, R. *Angew. Chem., Int. Ed.* **2002**, *41*, 3823−3825.
(77) Glaser, T. *Chem. Commun.* **2011**, *47*, 116−130.
(78) Glaser, T.; Heidemeier, M.; Krickemeyer, E.; Bögge, H.; Stammler, A.; Fröhlich, R.; Bill, E.; Schnack, J. *Inorg. Chem.* **2009**, *48*, 607−620.
(79) Albores, P.; Slep, L. D.; Baraldo, L. M.; Baggio, R.; Garland, M. T.; Rentschler, E. *Inorg. Chem.* **2006**, *45*, 2361−2363.
(80) Beauvais, L. G.; Long, J. R. *J. Am. Chem. Soc.* **2002**, *124*, 2110−2111.
(81) Desplanches, C.; Ruiz, E.; Alvarez, S. *Eur. J. Inorg. Chem.* **2003**, 1756−1760.
(82) Shores, M. P.; Sokol, J. J.; Long, J. R. *J. Am. Chem. Soc.* **2002**, *124*, 2279−2292.
(83) Zhang, Y.-Q.; Luo, C.-L. *Int. J. Quantum Chem.* **2006**, *106*, 1551−1560.
(84) Freedman, D. E.; Jenkins, D. M.; Long, J. R. *Chem. Commun.* **2009**, 4829−4831.
(85) Berlinguette, C. P.; Galán-Mascarós, J. R.; Dunbar, K. R. *Inorg. Chem.* **2003**, *42*, 3416−3422.
(86) Palii, A. V.; Reu, O. S.; Ostrovsky, S. M.; Klokishner, S. I.; Tsukerblat, B. S.; Hilfiger, M.; Shatruk, M.; Prosvirin, A.; Dunbar, K. R. *J. Phys. Chem. A* **2009**, *113*, 6886−6890.
(87) Dreiser, J.; Pedersen, K. S.; Schnegg, A.; Holldack, K.; Nehrkorn, J.; Sigrist, M.; Tregenna-Piggott, P.; Mutka, H.; Weihe, H.; Mironov, V. S.; Bendix, J.; Waldmann, O. *Chem.—Eur. J.* **2013**, *19*, 3693−3701.
(88) Curtis, J. C.; Meyer, T. J. *Inorg. Chem.* **1982**, *21*, 1562−1571.
(89) Macartney, D. H. *Inorg. Chem.* **1991**, *30*, 3337−3342.
(90) Wieghardt, K.; Schmidt, W.; Herrmann, W.; Kuppers, H. J. *Inorg. Chem.* **1983**, *22*, 2953−2956.
(91) Sheldrick, G. M. *SADABS 2008/1*; University of Göttingen: Göttingen, Germany, 2008.
(92) Sheldrick, G. M. *Acta Crystallogr.* **2008**, *A64*, 112−122.
(93) Palii, A.; Tsukerblat, B.; Klokishner, S.; Dunbar, K. R.; Clemente-Juan, J. M.; Coronado, E. *Chem. Soc. Rev.* **2011**, *40*, 3130−3156.
(94) van Wüllen, C. *Mol. Phys.* **2013**, *111*, 2392−2397.
(95) Schnack, J. *Condens. Matter Phys.* **2009**, *12*, 323−330.
(96) Krickemeyer, E.; Hoeke, V.; Stammler, A.; Bögge, H.; Schnack, J.; Glaser, T. *Z. Naturforsch.* **2010**, *65b*, 295−303.
(97) Feldscher, B.; Krickemeyer, E.; Moselage, M.; Theil, H.; Hoeke, V.; Kaiser, Y.; Stammler, A.; Bögge, H.; Glaser, T. *Sci. China: Chem.* **2012**, *55*, 951−966.

(98) Freiherr von Richthofen, C.-G.; Feldscher, B.; Lippert, K.-A.; Stammler, A.; Bögge, H.; Glaser, T. *Z. Naturforsch.* **2013**, *68b*, 64−86.
(99) Helmstedt, A.; Sacher, M. D.; Gryzia, A.; Harder, A.; Brechling, A.; Müller, N.; Heinzmann, U.; Hoeke, V.; Krickemeyer, E.; Glaser, T.; Bouvron, S.; Fonin, M. *J. Electron Spectrosc. Relat. Phenom.* **2012**, *184*, 583−588.
(100) Freiherr von Richthofen, C.-G.; Stammler, A.; Bögge, H.; DeGroot, M. W.; Long, J. R.; Glaser, T. *Inorg. Chem.* **2009**, *48*, 10165−10176.
(101) Cavallo, L.; Jacobsen, H. *Eur. J. Inorg. Chem.* **2003**, 892−902.
(102) Kruszewski, J.; Krygowski, T. M. *Tetrahedron Lett.* **1972**, *6*, 3839−3842.
(103) Krygowski, T. M.; Cyranski, M. K. *Chem. Rev.* **2001**, *101*, 1385−1419.
(104) Krygowski, T. M.; Cyranski, M. K. *Phys. Chem. Chem. Phys.* **2004**, *6*, 249−255.
(105) Feldscher, B.; Stammler, A.; Bögge, H.; Glaser, T. *Dalton Trans.* **2010**, *39*, 11675−11685.
(106) Feldscher, B.; Stammler, A.; Bögge, H.; Glaser, T. *Polyhedron* **2011**, *30*, 3038−3047.
(107) Freiherr von Richthofen, C.-G.; Stammler, A.; Bögge, H.; Glaser, T. *J. Org. Chem.* **2012**, *77*, 1435−1448.
(108) Strautmann, J. B. H.; Walleck, S.; Bögge, H.; Stammler, A.; Glaser, T. *Chem. Commun.* **2011**, *47*, 695−697.
(109) Walleck, S.; Theil, H.; Heidemeier, M.; Heinze-Brückner, G.; Stammler, A.; Bögge, H.; Glaser, T. *Inorg. Chim. Acta* **2010**, *363*, 4287−4294.
(110) Alexander, J. J.; Gray, H. B. *J. Am. Chem. Soc.* **1968**, *90*, 4260−4271.
(111) Boucher, L. J. *J. Inorg. Nucl. Chem.* **1974**, *36*, 531−536.
(112) Boucher, L. J.; Coe, C. G. *Inorg. Chem.* **1975**, *14*, 1289−1294.
(113) Boucher, L. J.; Coe, C. G. *Inorg. Chem.* **1976**, *15*, 1334−1340.
(114) Boucher, L. J.; Farrell, M. O. *J. Inorg. Nucl. Chem.* **1973**, *35*, 3731−3738.
(115) Boucher, L. J.; Herrington, D. R. *Inorg. Chem.* **1974**, *13*, 1105−1108.
(116) Gohdes, J. W.; Armstrong, W. H. *Inorg. Chem.* **1988**, *27*, 1841−1842.
(117) Dey, K.; De, R. L. *J. Inorg. Nucl. Chem.* **1977**, *39*, 153−155.
(118) Bellitto, C.; Tomlinson, A. A. G.; Furlani, C. *J. Chem. Soc. A* **1971**, 3267−3271.
(119) Girerd, J.-J.; Journaux, Y. In *Physical Methods in Bioinorganic Chemistry*; Que, L. J., Ed.; University Science Books: Sausalito, 2000; pp 321−374.
(120) Dunbar, K. R.; Schelter, E. J.; Palii, A. V.; Ostrovsky, S. M.; Mirovitskii, V. Y.; Hudson, J. M.; Omary, M. A.; Klokishner, S. I.; Tsukerblat, B. S. *J. Phys. Chem. A* **2003**, *107*, 11102−11111.
(121) Kahn, O. *Molecular Magnetism*; VCH Publisher: New York, 1993.
(122) Palii, A. V.; Tsukerblat, B. S.; Coronado, E.; Clemente-Juan, J. M.; Borrás-Almenar, J. J. *J. Chem. Phys.* **2003**, *118*, 5566−5581.
(123) Palii, A. V.; Ostrovsky, S. M.; Klokishner, S. I.; Tsukerblat, B. S.; Dunbar, K. R. *ChemPhysChem* **2006**, *7*, 871−879.
(124) Mironov, V. S.; Chibotaru, L. F.; Ceulemans, A. *Phys. Rev. B* **2003**, *67*, 014424.
(125) Atanasov, M.; Comba, T.; Daul, C. A. *Inorg. Chem.* **2008**, *47*, 2449−2463.